Lithos 112S (2009) 1096–1108

Contents lists available at ScienceDirect

Lithos

journal homepage: www.elsevier.com/locate/lithos

An integrated petrological, geochemical and Re–Os isotope study of peridotite xenoliths from the Argyle lamproite, Western Australia and implications for cratonic diamond occurrences

A. Luguet [a,b,*], A.L. Jaques [c], D.G. Pearson [a], C.B. Smith [d], G.P. Bulanova [e], S.L. Roffey [f], M.J. Rayner [g], J.-P. Lorand [h]

[a] Northern Centre for Isotopic and Elemental Tracing, Department of Earth Sciences, University of Durham, UK
[b] Steinmann Institut, Endogene Prozesse, Rheinische Freidrich-Wilhems-Universität Bonn, Germany
[c] Geoscience Australia, Canberra ACT, Australia
[d] Rio Tinto Mining and Exploration Ltd., London, UK
[e] University of Bristol, UK
[f] Rio Tinto Exploration Pty. Ltd., Perth, Australia
[g] Argyle Diamond Mines Ltd, West Perth, Australia
[h] Muséum National d'Histoire Naturelle, Laboratoire de Minéralogie et Cosmochimie, CNRS UMR 7202, Paris, France

ARTICLE INFO

Article history:
Received 7 October 2008
Accepted 11 May 2009
Available online 18 June 2009

Keywords:
Peridotite xenoliths
Lithosphere
Diamond
Craton
Re–Os dating
Mobile belt

ABSTRACT

An integrated study of the petrology and Re–Os geochemistry of a suite of peridotite xenoliths, some carrying abundant diamonds, from the richly diamondiferous Argyle AK1 lamproite pipe provides definitive evidence for a depleted lithospheric root of Neoarchean age (T_{RD} eruption ~2.2–3.1 Ga) beneath the Proterozoic Halls Creek Orogen at the margin of the Kimberley Craton, Western Australia. The microdiamonds from the peridotitic xenoliths are similar in their properties to the minor population of small, commercial sized, peridotitic diamonds from Argyle, both formed in the Archean from isotopically mantle-like carbon. The major element bulk chemistry and mineral chemistry of the Argyle peridotites are slightly less depleted than Archean cratonic peridotites as a whole but similar to those reported from Neoarchean–Paleoproterozoic cratonic provinces. The Argyle peridotite xenoliths were derived from within the diamond stability field (1050–1300 °C and 4.9–5.9 GPa) near the base of the lithosphere (typically 160–200 km depth) with a geothermal gradient of 41.5 mW/m^2. This thick diamondiferous lithosphere, estimated at up to 225 km thick from present day seismic S-wave tomography, appears to have persisted since the time of eruption of the Argyle lamproite (~1180 Ma).

The existence of late Archean age lithosphere beneath the Argyle diamond pipe, in a region where no crustal rocks of Archean age are known, suggests a decoupling of the crust and mantle in the region of the Halls Creek Orogen, perhaps as a consequence of Paleoproterozoic (~1.85 Ga) reworking and/or subduction at the margin of the Kimberley Craton. The confirmation of an Archean lithospheric root beneath the Argyle pipe at the margin of the Kimberley Craton seemingly conforms with "Clifford's Rule", regarding the restriction of economic diamond deposits to those underlain by Archean cratons. However, Argyle owes its rich diamond grades not to its Neoarchean mantle roots but to the presence of richly diamondiferous eclogitic material accreted to the craton root during the Proterozoic.

1. Introduction

The Argyle mine, one of the world's largest diamond mines, is the only major diamond deposit found in an early Proterozoic mobile belt. It is hosted by the Argyle AK1 lamproite pipe and lies within the Halls Creek Orogen (HCO) at the southeast margin of the Kimberley Craton in Western Australia (Fig. 1). Archean mobile belts such as the Limpopo Belt contain diamondiferous pipes (e.g. Venetia, River Ranch). However, with a few exceptions such as the Prairie Creek (USA) lamproite (Lambert et al., 1995), Buffalo Head Hills (Canada) kimberlites (Carlson et al., 1999), Pimenta Bueno and Juina (Brazil) kimberlites (Bulanova et al., 2008a,b), kimberlites and other alkaline ultrabasic volcanic rocks (including lamproites) intruding post-Archean mobile belts at the margins of cratons are mostly barren of diamonds, presumably having been derived from shallower depths and thus sampled lithosphere in the graphite stability field (Janse, 1994). A number of studies of the Southern African (Kalahari and

* Corresponding author. Steinmann Institut, Endogene Prozesse, Rheinische Freidrich-Wilhems-Universität Bonn, Germany. Tel.: +49 228 73 6816; fax: +49 228 73 2770.
E-mail address: ambre.luguet@uni-bonn.de (A. Luguet).

0024-4937/$ – see front matter © 2009 Elsevier B.V. All rights reserved.
doi:10.1016/j.lithos.2009.05.022

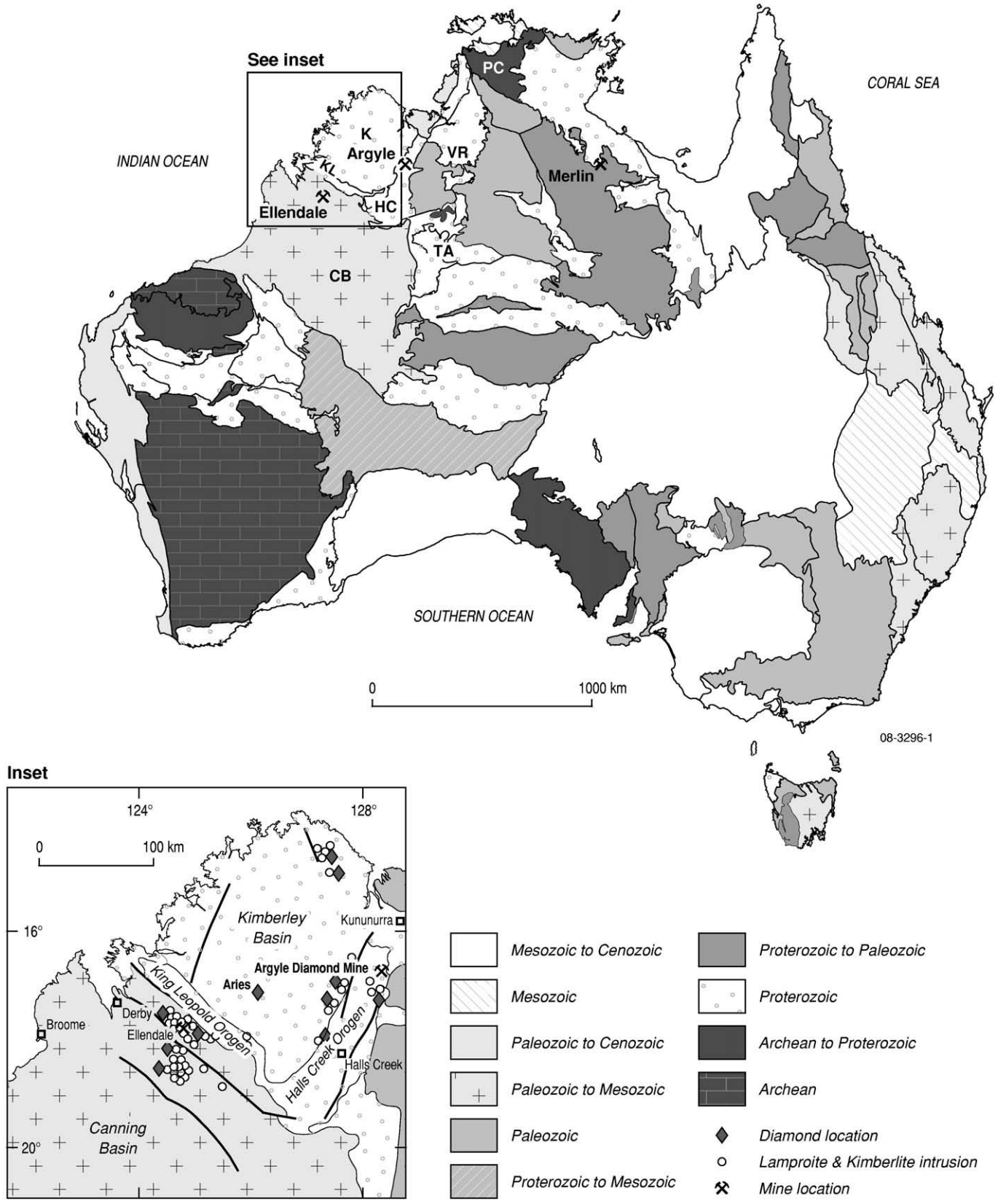

Fig. 1. Simplified geological map of Australia showing location of Argyle mine, the Halls Creek Orogen and the Kimberley Craton in relation to major geological regions by age. The inset shows the distribution of kimberlites and lamproites in the Kimberley Craton and the Argyle and Ellendale diamond mines. CB=Canning Basin, K=Kimberley Craton, PC=Pine Creek Inlier, TA=Tanami Province, and VR=Victoria River Basin.

Kaapvaal) Craton, the Siberian and North Atlantic Cratons, have demonstrated a general correspondence between the age of the crust and the age of its underlying mantle (e.g. Carlson et al., 2005 and refs. within) and provided compelling evidence that cratonic lithospheric mantle is typically coupled with its overlying crust (Helmstaedt, this issue). It is therefore important to constrain the depth and the age of

the lithosphere beneath the Argyle pipe both from the point of view of understanding the occurrence and origin of diamonds, and in terms of constraining the geometry of the Archean cratonic root at depth and hence craton-mobile belt assembly models in general (Rudnick and Walker, this issue).

Previous thermobarometry (Jaques et al., 1990) showed that peridotite xenoliths, both diamondiferous and non-diamondiferous, from the Argyle pipe were equilibrated within the diamond stability field (1140–1290 °C, 5–5.9 GPa), corresponding to depths of 160–190 km, similar to the range typically reported for diamondiferous and 'diamond-facies' peridotites from kimberlite pipes. This implies a lithosphere thickness of up to 200 km, comparable with estimates from present day S-wave tomographic models that suggest that the Kimberley craton is underlain by a thick (up to 250 km) lithospheric root that thins to the east and south (Van der Hilst et al., 1998; Kennett, 2003; Fishwick et al., 2005). Jaques and Milligan (2004) suggested that the location of the Argyle pipe (and other diamondiferous intrusions) coincides with the edge of a (old) thick lithospheric root beneath the Kimberley Craton.

Here we present Re–Os analyses on a suite of 23 peridotite xenoliths based on a substantial new collection of mantle xenoliths from the Argyle lamproite pipe. The study integrates petrologic, geochemical and Re–Os age data to define the nature and age of the deep lithospheric root to the richly diamondiferous Argyle diamond mine at the time of lamproite intrusion.

2. Regional geology

The Mesoproterozoic (~1180 Ma) Argyle AK1 olivine-lamproite pipe intrudes the eastern edge of the NNE-trending Paleoproterozoic HCO, which lies between the Kimberley Craton in the west and the other components of the North Australian Craton to the east (Fig. 1). The HCO is intruded by a number of lamproite and ultramafic lamprophyre bodies, some of which carry diamonds (Jaques et al., 1986), but Argyle is the only economic intrusion. Details of the geology of the pipe are given by Boxer et al. (1989) and of the geochemistry by Jaques et al. (1989a).

The HCO comprises three north-northeasterly-trending basement terranes containing weakly to strongly deformed and metamorphosed Paleoproterozoic sedimentary, volcanic and intrusive rocks including voluminous granites and several suites of layered mafic-ultramafic intrusions (Hoatson and Blake, 2000). Major deformations affected the westernmost zone of the HCO between 1865 and 1850 Ma (Hooper Orogeny), the central zone between 1863 and 1845 Ma, and both the central and eastern zones between 1835 and 1805 Ma (Halls Creek Orogeny). Post-1800 Ma sedimentary basins occur in all three zones. Later intracratonic deformation events variably affected the rocks of the HCO at ~1000 Ma (Yampi Orogeny), ~560 Ma (King Leopold Orogeny) and ~300 Ma (Alice Springs Orogeny).

The age of the lithosphere underlying the Kimberley Craton, the HCO, and the North Australian Craton is poorly constrained. Hancock and Rutland (1984) and Etheridge et al. (1987) postulated a common Archean substrate for all three crustal elements. Subsequent geological and geophysical studies suggest that the HCO represents a plate boundary between the two cratonic blocks (e.g. Myers et al., 1996; Sheppard et al., 1999; Shaw et al., 2000; Betts et al., 2002). In the eastern zone of the HCO, ~1910 Ma volcanic rocks are unconformably overlain by a fluviatile sandstone that yielded detrital zircon ages lying exclusively within the 2.4–3.6 Ga range (Tyler et al., 1999), suggesting the presence of Archean basement. In the central HCO, Sm-Nd model ages for the Argyle lamproite indicate that the lamproite was derived from, or at least includes, an ancient enriched component, implying mantle of early Proterozoic to late Archean age (>2 Ga, Jaques et al., 1989a). Graham et al. (1999) reported Re–Os data for two Argyle peridotite xenoliths that indicated an apparent Archean age (>2.55 Ga) for the mantle root under Argyle. However, the T_{Ma} ages calculated by Graham et al. (1999) are likely to overestimate the actual age of depletion of the mantle root since the Re contents of the 2 studied xenoliths obviously bear metasomatic imprints. Finally, within the Kimberley Craton, Downes et al. (2007) reported Hf isotope compositions for Paleoproterozoic (1850 Ma, U–Pb date) zircons in peridotite xenoliths from the Neoproterozoic (~820 Ma) Aries kimberlite in the southern Kimberley Craton (Fig. 1) that have late Archean Lu–Hf model ages.

3. Samples and methods

A number of mantle peridotite xenoliths have been exclusively recovered from the low diamond grade 'non-sandy' tuff member at the northern end of the pipe. A suite of 71 peridotite xenoliths, including 7 diamond-bearing peridotites, recovered during the first years of mining was described by Jaques et al. (1990). Surprisingly, no eclogite xenoliths were encountered despite abundant eclogitic silicate inclusions within the Argyle diamonds (Hall and Smith, 1984; Jaques et al., 1989b). Mining activity in 2003 revealed a new zone within the 'non sandy' tuff member (Boxer et al., 1989) of the lamproite intrusion where mantle xenoliths, in various states of preservation, were concentrated. Efforts by the mine staff led to the recovery of several hundred new peridotite xenoliths that form the basis of this study.

3.1. Sample selection and microdiamond determination

The xenoliths are all oblate to disc-shaped, range in size from 8 to 12 cm and typically weigh between 0.4 and 0.8 kg, the largest weighing 1.1 kg. They commonly display a strong reaction rim with the host lamproite. From the several hundred samples collected more than 100 were examined in thin section using transmitted and reflected light petrographic microscopy and 69 of these were also examined in thick section, photographed digitally and imaged by SEM equipped with an energy dispersive analyzer. Samples were selected for mineral and whole-rock geochemistry on the basis of the petrographic studies (least alteration, presence of relic primary phases, and absence of lamproite micro-veinlets) and sample size. Following these criteria, a total of 23 peridotite xenoliths – 19 recently discovered xenoliths and 4 well-characterized peridotite xenoliths from the original suite (Jaques et al., 1990) – were chosen for mineral and whole-rock geochemistry. On those selected samples, all the visible reaction zones with the lamproite and alteration rims were removed in order to preserve only the fresher dark-green zones. Up to 100 g of rock powders were prepared for major, trace and ultra-traces (i.e. Re and Os) analyses, starting from 100–200 g sample masses. Petrographic details are given in Table 1.

Chromite separates were prepared from peridotite xenolith 6504257 by crushing and heavy liquid separation. Chrome spinels were hand picked from the concentrates under the binocular microscope and divided by morphological appearance into primary chrome-rich types with characteristic anhedral, larger shapes (fractions A and B) and Al–Cr symplectite spinels (fractions C and D) which form much smaller equant shapes (see Section 4.1 below).

Finally, portions of 20 xenoliths were fused with caustic soda for extraction of microdiamonds. Three small monocrystalline diamonds 0.7 mm in size were then polished down to expose mineral inclusions for analysis.

3.2. Microbeam analysis

Mineral analyses were carried out by wavelength dispersive methods using a Cameca SX-100 electron probe micro-analyser (EPMA) at the Research School of Earth Science, Australian National University, using methods and detection limits very similar to those reported by Jaques et al. (1990) except that detection limits are lower for Ca and Al (50, 70 ppm respectively) and higher for K (130 ppm) in this study. Between 5 and 10 analyses of each phase were undertaken. Representative analyses are given in Table A Appendix A. EPMA analyses of major elements and laser ablation mass spectrometer (LA-MS) analyses of trace elements for spinels from Argyle xenoliths 6504257

Table 1
Petrography of Argyle peridotite xenolith samples analysed.

Sample		Ol	Opx	Cpx	"Ga"	Cr	alteration	Primary minerals
6504010		X	X	?x	x	–	++/+++	Relic Ol, Opx
6504022		**X**	**X**	**x**	x	–	+++	Relic Ol, Opx, Cpx
6504049	◆	X	X	?x	x	–	+++	No
6504051		X	X	**x**	x	–	+++	Relic Cpx
6504062		X	X	**x**	x	–	+++	Relic Cpx
6504072		**X**	**X**	**x**	x	–	++	Abundant relic Ol, Opx, Cpx
6504078		X	X	**x**	x	–	+++	Relic Cpx
6504091		**X**	**X**	?x	x	–	+++	Abundant relic Ol, Opx
6504093		**X**	**X**	?x	x	–	+++	Relic Ol, Opx
6504096		**X**	**X**	**x**	x	–	+++	Relic Ol, Opx, Cpx
6504111		X	X	?x	x	–	+++	No
6504131	◆	**X**	**X**	?x	x	–	+++	Rare relic Ol, Opx
6504138		**X**	**X**	x	x	–	+++	Relic Ol, Opx
6504142		X	X	x	x	–	+++	No
6504148	◆	**X**	**X**	**X**	x	–	++	Abundant relic Ol, Opx, Cpx
6504149	◆	**X**	**X**	?x	x	–	++	Relic Ol, Opx
6504158		X	X	?x	x	–	+++	No
6504180		X	X	**x**	x	–	+++	Relic Cpx
6504221		**X**	**X**	?x	x	–	+++	Relic Ol, Opx
6504256		X	X	?x	x	–	+++	No
6504257		X	X	?x	x	**x**	+++	Chromite
6504270	◆	X	X	?x	x	–	+++	No
6504271	◆	X	X	**x**	x	–	+++	Relic Cpx
6504293		X	X	**x**	x	–	+++	Rare relic Cpx
6504294		X	X	?x	x	–	+++	No
N23[a]		**X**	**X**	**x**	x	–	+/++	Abundant relic Ol, Opx, Cpx
N25[a]		**X**	**X**	?x	x	–	++	Abundant relic Ol, Opx
N40[a]	◆	**X**	**X**	**x**	x	–	+/++	Abundant relic Ol, Opx, Cpx
N48[a]		**X**	**X**	**x**	x	–	++	Abundant relic Ol, Opx

Diamond symbol=diamondiferous peridotites. X = major phase, x = minor phase, ?x = primary phase inferred but not confirmed because of extensive alteration. Bold indicates relic primary phases analysed by electron microprobe. Ol = olivine, Opx = orthopyroxene (enstatite), Cpx = clinopyroxene (Cr-diopside), "Ga" = former garnet now replaced by spinel-rich symplectite, Cr = chromite.
[a] From Jaques et al. (1990).

and N45 were undertaken at University of Bristol. EPMA analyses were made with a Cameca SX100 microprobe. LA-MS analyses used a Merchantek/New Wave Research MicroProbe II frequency quadrupled Nd:YAG 266 nm UV laser ablation system, coupled to a Thermo Elemental PlasmaQuad 3 ICP-MS equipped with both a standard ion-sampling interface and an S-Option high efficiency interface.

3.3. Geochemistry techniques

Major elements were analysed for the 19 recently-discovered peridotite xenoliths by X-ray fluorescence at the University of Cape Town, South Africa. Trace elements were determined by ICP-MS at Durham University using a Perkin Elmer Sciex Elan 6000 quadrupole ICP-MS. Replicate analyses of international reference material (BIR-1, W2, BHVO-1, AGV-1, BE-N, SRM 688) and in-house reference material (GP13, Beni-Bousera garnet-lherzolite) agree well with the recommended values. Reproducibility and precision estimated from these duplicate analyses are better than 6% (2σ) and within 90% respectively for the elements reported in Table B Appendix A.

Os concentrations and $^{187}Os/^{188}Os$ ratios were determined using the Thermo-Finnigan N-TIMS of the University of Durham. Re concentrations were determined by isotope dilution inductively coupled plasma mass spectrometry, using the Thermo-Finnigan Element 2 ICP-MS of the University of Durham. Prior to measurements, sample digestions were performed with 7.5 mL inverse aqua regia on 1 g of whole-rock sample powder aliquot and on 5–15 mg chromite separates (fractions A and B) at moderate temperature (220 °C) and moderate pressure in glass Carius tubes for at least 24 h. For several samples, digestions of 1 to 2 grams of whole-rock powder and of 3–37 mg of chromite separates (fractions C and D) were duplicated using the Anton-Paar high pressure-asher. Digestion runs were in this case performed at 300 °C and 100 bars for at least 4 h. High-pressure dissolution methods have been shown to attack better and therefore more effectively dissolve the refractory minerals (e.g. alloys) potentially hosting osmium (Meisel and Moser, 2004). Details of the chemical separation for Os and Re are provided in Pearson and Woodland (2000) and Pearson et al. (2004). Total procedural blanks and analyses of international standard samples have been carried out by the two digestion techniques. The procedural blanks vary between 1–2 ppt Os and 1.4–4.5 ppt Re for the Carius-Tube dissolution (N = 2) and 0.2–0.7 ppt Os and 3.4–5 ppt Re using the high-pressure dissolutions (N = 2). The average procedural blanks obtained by HT-HP digestion are systematically better for Os. Replicate analyses of in-house standard sample (GP-13) performed by carius tube dissolution (N = 2) yield reproducibility of 5–6% for Os and 14–17% for Re. Rhenium reproducibility becomes better when analyses are done using high temperature-high pressure digestions (1.5%). When compared with analyses performed using similar digestion methods (Meisel and Moser, 2004), precision of our in-house standard GP13 is better than 5% for Os and 9% for Re for Carius Tube dissolutions and is highly improved when performing HP-Asher dissolutions (<5% for Re, 9–11% for Os). Reproducibility of $^{187}Os/^{188}Os$ ratios for TIMS analyses in Durham University ranges from 0.8 to 1.4‰, similar to the long-term reproducibility of the University of Maryland standard solution (2‰ over 3 years).

4. Mineralogy and petrology of Argyle peridotite xenoliths

4.1. Textures and mineral assemblages

The xenoliths show various states of preservation ranging from samples where no primary silicates remain to those that still contain relic olivine and pyroxenes, allowing thermobarometry estimates (Jaques et al., 1990). Relic primary assemblages and preserved textures indicate that the xenoliths were mostly garnet lherzolites with coarse grains (typically 1–4 mm) of olivine, orthopyroxene, and subordinate amounts of clinopyroxene and former garnet. Summary petrographic data are given in Table 1. All xenoliths have undergone only mild to moderate deformation exhibited by the presence of undulose extinction, kink-bands, and deformation lamellae. In the more deformed samples, the enstatite grains have a weak porphyroclastic texture. Although not found in all samples, the absence of highly refractory olivine and Ca-poor enstatite (see below) suggests that chrome diopside is likely present in all samples, even in small amounts. Olivine is replaced to varying extents by lizardite, montmorillonite, and talc, and pyroxenes by talc, calcite and/or tremolite (diopside), whereas garnets have been entirely replaced by symplectic intergrowths of fine-grained Al–Cr spinel, pyroxene and secondary silicates showing a large variety of textures. Fine-grained dense intergrowths typically preserve the shape of the former garnet. In more open-textured symplectites, the core of the former garnet is entirely replaced by secondary silicates and the former rim is defined by equant euhedral grains (up to 100 μm, but typically 20-60 μm) of Cr-Al spinel (Jaques et al., 1990). Rare Cr-rich chromite also occurs in a few samples as discrete sub- to anhedral interstitial grains 50–300 μm across commonly with cuspate margins and fractured, some elongated in shape. Some are spatially associated with the former garnets (now symplectites).

4.2. Diamonds

Diamonds were found in 14 of the 69 xenoliths processed (8 in the original suite and 6 in the newly discovered xenoliths). Details of stones recovered and sample weights processed from the newly discovered suite are listed in Table C Appendix A. Diamond presence in both suites is highly erratic and spotty, with number of stones per xenolith varying from 0 to 158. The diamond grade of individual diamondiferous xenoliths (including those studied by Jaques et al., 1990) ranges from <0.001 ct/t to 333 ct/t, with an average grade of 31.48 ct/t. The overall grade, including the barren peridotite xenoliths, is 24.34 ct/t.

The stones are generally microdiamonds <0.4 mm in diameter with few larger than 0.7 mm. They are irregular unresorbed octahedra,

macled octahedra, aggregates, and broken stones (Hall and Smith, 1984; Trautman, 1999), colourless, very pale grey, brown or yellow in colour, often with deeply frosted surfaces coated with graphite. These diamonds are similar to small un-resorbed and etched octahedral diamonds of peridotitic paragenesis, which form 5% only of Argyle commercial production (Hall and Smith, 1984; Jaques et al., 1989b). The bulk of the Argyle commercial stones (95%) are mostly strongly coloured and heavily resorbed dodecahedra of eclogitic paragenesis and differ sharply in morphology from the peridotite xenolith microdiamonds.

Two diamonds from xenoliths analysed by FTIR do not contain nitrogen and are Type II (this study); Trautman (1999) undertook FTIR investigations of the original xenolith microdiamond suite and found N contents varied from 71–112 ppm with most diamonds having >85% IaB aggregation. Carbon isotope measurements made on the original xenolith microdiamond suite ranged from −1 to −5 δ^{13}C‰ (Trautman, 1999), slightly heavier than average mantle values (−5.5 δ^{13}C ‰) as given by Deines (2002).

Very small inclusions in the peridotite xenolith microdiamonds were identified as tiny black graphite spots or Ni-rich sulfides by SEM analysis. A single olivine inclusion ($Mg^{\#}_{92.6}$ where $Mg^{\#} = 100*Mg/(Mg+Fe)$), was also found.

4.3. Base metal sulfides

Despite detailed scrutiny, no mantle-derived base metal sulfides (BMS) have been observed in any of the Argyle xenoliths examined but some contain hydrothermal (secondary) BMS as 'accessory' minerals. These occur in two populations. The first population occurs as tiny (20–50 μm long), euhedral Co-rich-Ni-pentlandite (up to 6.2 wt.% Co) ± heazlewoodite grains disseminated within the serpentine matrix. Because of their small size, euhedral shape and their ubiquitous association with serpentinisation minerals, these sulfides are interpreted to have formed during serpentinisation as found in other studies of mantle peridotite (e.g., Philipidis, 1982; Luguet, 2000; Klein and Bach, 2009). The second population – comprising galena, chalcopyrite and pyrite – occurs as sulfide veinlets, sometimes showing a spongy texture and crosscutting both the serpentine and the bastite pseudomorphs. This sulfide paragenesis likely reacted with the serpentine matrix to form veinlet rims of Ni-pentlandite. Both hydrothermal sulfide generations have experienced oxidation as shown by the high O content of pentlandite and galena. In the case of pentlandite, this oxidation also leads to replacement by millerite and violarite.

4.4. Mineral chemistry

Olivine compositions are Mg-rich ($Mg^{\#}_{91.5–92.5}$), have high Ni contents and very low Ca (typically 300–400 ppm). Multiple analyses indicate that olivine grains within a single peridotite are uniform in composition, lying typically within analytical error. There is no difference in olivine composition between the diamondiferous and non-diamondiferous Argyle peridotite xenoliths. Compositions (Table A Appendix A) lie within the range found previously for Argyle peridotite xenoliths ($Mg_{91.2–93.1}$, Jaques et al., 1990) and have similar modes ($Mg_{91.7}$ cf $Mg_{91.9}$). These compositions are typical of moderately refractory mantle peridotite and comparable with olivine from cratonic peridotites world-wide (e.g. Pearson and Wittig, 2008).

The olivine inclusion in diamond recovered from xenolith sample 6,504,131 is also rich in Ni (0.38 wt.%) and Mg ($Mg^{\#}_{92.6}$) within error of the olivine in this xenolith ($Mg^{\#}_{92.4}$) and within the range previously found for olivine inclusions in Argyle diamonds ($Mg^{\#}_{92.4–94.5}$). The $Mg^{\#}$ values for olivines included in Argyle diamonds extend to higher, more refractory values than for olivine from the peridotite xenoliths (Jaques et al., 1990).

Enstatites also show a limited range in $Mg^{\#}$ (92.4–93.6), and have very low Al_2O_3 (0.4–0.8 wt.%) and CaO (0.6–1.2 wt.%) contents (Table A Appendix A). They also have uniformly low Ti contents (<0.06 wt.% TiO_2), contain significant Cr (0.2–0.35 wt.% Cr_2O_3) and have detectable Na (up to 0.17 wt.% Na_2O). They fall within the compositional range of those found previously at Argyle except for Al_2O_3 contents, which extend the range to slightly higher values. The very low Al_2O_3 contents are typical of enstatite compositions found in diamondiferous peridotites and inclusions in diamond and, when coexisting with garnet, indicate equilibration at very high pressures.

Chrome diopsides have uniformly high Mg# and Ca with Ca/(Ca + Mg + Fe) in the range 0.39–0.44. All have low contents of Al_2O_3 (0.7–1.5 wt.%), Na_2O (0.6–1.3 wt.%) and TiO_2 (typically <0.1 wt.%, Table A Appendix A). As reported by Jaques et al (1990), some clinopyroxene grains contain detectable amounts of K_2O. There is no apparent correlation of the K_2O content with the diopside composition. The major element composition of chrome diopside in the diamondiferous samples is very similar to that in the non-diamondiferous samples.

Picrochromite is rare and occurs as interstitial grains ranging from 200 μm to 1.5 mm in length in sample 6504257. Compositions are uniformly magnesian and chrome-rich (14–15 wt.% MgO, 56–58 wt.% Cr_2O_3, Cr# = (Cr/(Cr + Al) = 0.71–0.75) and very poor in Ti (typically at or below the detection limit: 0.02 wt.% TiO_2; Table A Appendix A). The chromite chemistry is comparable with that reported previously for 'primary chromite' in Argyle peridotite xenoliths (Jaques et al., 1990) and similar to but less refractory than chromite inclusions in diamonds and chromite in diamondiferous harzburgites (e.g. Sobolev et al., 1984; Stachel and Harris, 2008). Jaques et al. (1990) interpreted the chromites to be 'primary' in origin based on their textures, grain size and chemistry (very low Ti and uniformly high Mg and Cr contents) which are distinctly different from those of the symplectic Al–Cr spinels. However, the spatial association with the former garnet (now replaced by symplectite) might indicate a more complex origin for the chromite, perhaps involving recrystallisation from former Cr-rich garnet and/or metasomatism in the mantle.

Secondary Cr-Al spinels, together with Al-rich pyroxenes, occur in the symplectites as a breakdown product of garnet. These are distinguished from the coarse chromites by size, shape and chemistry. The symplectite spinels are invariably much smaller (<100 μm), typically euhedral, equant grains, and differ from the 'primary' spinels in having a wide range in Cr and Al contents (Cr# = 0.18–0.56; Jaques et al., 1990); all have high $Mg^{\#}$ consistent with high crystallisation temperatures.

5. Pressure-temperature estimates

Temperatures and pressures of equilibration of the primary silicate assemblage have been estimated using the Nimis and Taylor (2000) single pyroxene thermobarometer (NT2000) for 10 of the geochemical samples (Table D Appendix A). Data are also included for 4 other Argyle peridotite samples that preserve diopside but were considered unsuitable for geochemical analysis because of alteration and microveining. The NT2000 thermobarometer is based on the solubility of enstatite in diopside (temperature) and the solubility of Cr in diopside (pressure). For the Argyle samples, this thermobarometer yields temperatures between ~1050 and 1300 °C and pressures in the range 4.9–5.9 GPa (Fig. 2). This range is similar to the estimates of 1140–1290 °C and 5–5.9 GPa) reported previously by Jaques et al. (1990) based on the two-pyroxene thermometer and Al-in-opx and Ca-in-olivine barometers of Brey and Kohler (1990). Equilibration temperatures (1100–1220 °C) similar to those of the silicate phases were estimated for the primary chromites in samples 6504257 and N45 using the Ni–Mn and Ni–Co (Denny, 1998) geothermometers. According to time-temperature-N aggregation relationships (Evans and Harris, 1989), the high aggregation state recorded by Trautman (1999) for diamonds recovered from the earlier set of Argyle peridotite xenoliths implies high

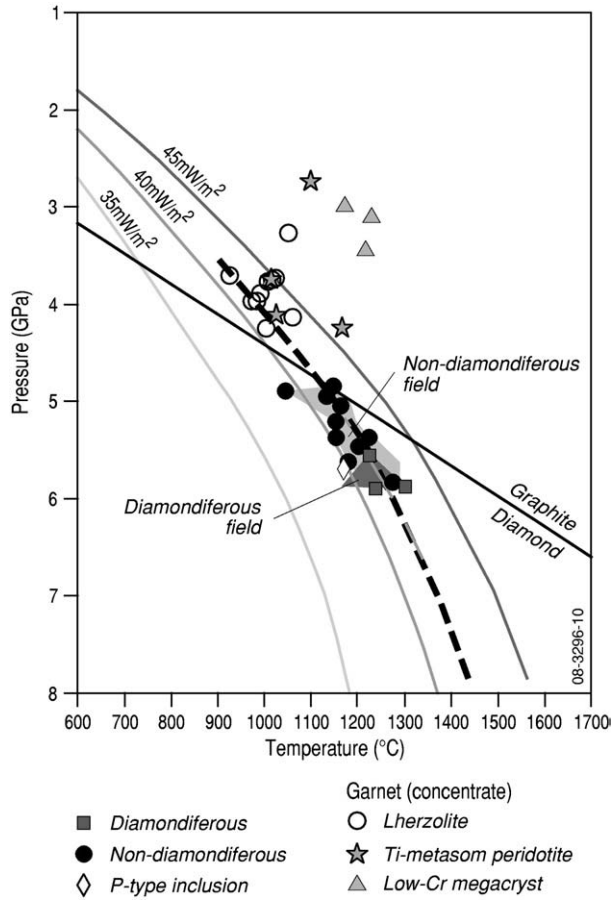

Fig. 2. Pressure-temperature estimates for Argyle peridotite xenoliths based on Nimis and Taylor (2000) clinopyroxene thermobarometry (this study) compared with conductive 35, 40 and 45 mW/m^2 geotherms and fields for all Argyle peridotite xenoliths and the diamondiferous peridotite xenoliths (this study and Jaques et al., 1990). Also plotted is a single Cr-pyrope inclusion in Argyle diamonds and PT estimates for other Cr-bearing garnets (see text).

mantle storage temperatures of some 1250–1300 °C for mantle residence times of between 1 and 3 Ga. This is in general agreement with the thermometry results calculated from the silicate assemblages and chromite above, and agrees especially with results from the diamondiferous xenoliths (Fig. 2).

The thermobarometry indicates that the Argyle lamproite sampled moderately depleted but diamondiferous lithosphere at depths of 150–200 km with a geothermal gradient of ~41.5 mW/m^2. A single Cr-rich (14.6 wt.% Cr_2O_3) pyrope inclusion from a peridotitic Argyle diamond plots close to the P-T field defined by Argyle diamondiferous peridotites (pressure: Cr in garnet using Grütter et al., 2006; temperature by olivine-garnet Fe-Mg using O'Neill and Wood, 1979) whereas low-Cr lherzolitic garnets (≤wt.6% Cr_2O_3, CaO) from Argyle concentrate fall within the graphite stability field based on the Ni-in-garnet thermometer (Canil, 1999) and Cr-in-garnet barometer (Ryan et al., 1996). The secondary spinels in the symplectites record a much wider range of crystallisation temperatures from quasi-magmatic or equivalent to the primary phases through to lower temperatures (800–1000 °C), which, if accurate, are likely to be sub-solidus or cooling temperatures.

6. Whole rock major element and trace element compositions

6.1. Major elements

All the Argyle peridotites analysed for our study are coarse-grained garnet-lherzolites and garnet-harzburgites, which have experienced extensive alteration (LOI = 9–19 wt.%, Table B Appendix A). Argyle peridotites are characterized by low Al_2O_3 (0.56–1.95 wt.%), TiO_2 (0.06–0.29 wt.%), CaO (0.19–2.30 wt.%) and Na_2O (<0.28 wt.%) contents consistent with the moderately to strongly refractory composition of the major minerals. The CaO versus Al_2O_3 systematics are similar to those observed for cratonic peridotites. The Argyle peridotites also overlap the composition of the most refractory off-craton peridotitic xenoliths (Fig. 3). This trend, and the overall refractory major element chemistry of the Argyle peridotite xenoliths, is typical of residues of partial melting with concentrations of magmaphile elements decreasing from lherzolite to harzburgite. This relation shows however some scatter which could be partly due to disturbance of CaO by secondary processes (e.g. carbonate precipitation in sample 6504256 as suggested by both high Ca and high Sr contents). On the other hand, Argyle peridotites have higher SiO_2 contents (44–53 wt.%) than reported so far for peridotite massifs and xenoliths whether from cratonic or off-craton settings. When plotted against MgO contents, the Argyle peridotites define a negative trend, similar to and overlapping the one observed for the other cratonic peridotites as well as fore-arc peridotites. This trend is nevertheless distinct from the trend defined by both the massif peridotites (Pyrenees, Lanzo, Ronda), and the off-craton xenoliths (e.g. Kilbourne Hole, SE Australia, Massif Central France, Ethiopia) for which only smaller variations of SiO_2 contents are generally observed for the same MgO variations (see for example. Bedini et al, 1997; Lorand et al., 1999; Zangana et al., 1999).

6.2. Trace elements

Transition element concentration ranges of the studied samples are generally similar to those reported for massifs and peridotite xenoliths (Table B Appendix A). Abundances of nickel, scandium and vanadium, three mildly incompatible elements hosted respectively by olivine and clinopyroxene, plot within the field of cratonic peridotites and display overall correlation with the degree of depletion (expressed as Al_2O_3) characteristic of partial melting residues. Seven peridotites nevertheless show higher V contents for a given depletion degree (Canil, 2004). Chromium abundances display a weak positive correlation with Al_2O_3 contents ($r = 0.65$), as systematically observed for cratonic peridotites containing less than 2 wt.% Al_2O_3. The weakness of the relationship is likely due to the 'nugget effect' related to the small size of the Argyle xenoliths and the heterogeneous distribution of spinel and chromite at the hand-specimen scale.

Abundances of large ion lithophile elements (LILE), rare earth elements (REE) and high field strength elements (HFSE) have been

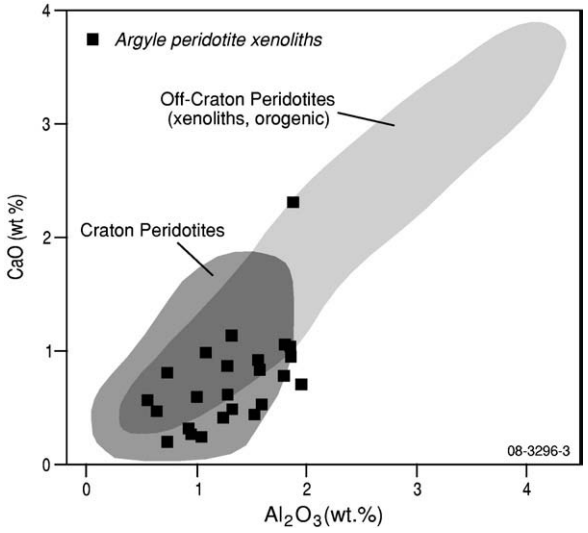

Fig. 3. Comparison of CaO and Al_2O_3 contents of Argyle peridotite xenoliths with peridotite xenoliths from cratonic and non-cratonic areas (Lorand et al., 1999; Lee, 2002; Irvine et al., 2003; Pearson et al., 2004).

determined for the lamproite by analyzing the host rock of the xenolith sample 6504149 as well as the 23 peridotites. The host rock has an incompatible element-enriched trace pattern similar to the Argyle olivine-lamproite dykes (Jaques et al., 1989a) with high La_N/Yb_N (~82) and high concentrations of Ba, La, Sr and Zr relative to estimated abundances of the primitive mantle (Ba_{PM} = 92, La_{PM} = 188, Sr_{PM} = 34, Zr_{PM} = 53; PM = primitive mantle normalized after McDonough and Sun, 1995). The concentration range of the LILE, REE and HFSE in the Argyle peridotites is 0.06–350 times that of primitive mantle. The observed enrichments in incompatible trace elements are inconsistent with the major element depletion and the refractory mineral compositions. The chondrite-normalized REE patterns display a negative slope (La_N/Yb_N = 10–370) reflecting a strong enrichment in light REE closely mimicking the REE pattern of the lamproite (Fig. 4). Abundances of the LREE and the medium REE vary sympathetically (i.e. Sm versus La): this is inferred to be a result of lamproite addition by infiltration. In contrast, the heavy REE do not co-vary with the LREE suggesting that the HREE concentrations are minimally disturbed and likely preserve melting trends (e.g., Canil, 2004; Wittig et al., 2008). Ytterbium abundances display a weak positive correlation with Al_2O_3 for 18 samples (r = 0.56) while 6 samples show slight to strong enrichment in Yb for a given Al_2O_3 content. Ytterbium is well known to be a very compatible element whose behavior and concentrations depend on the pressure and conditions of melting (Walter, 2003; Canil, 2004). Ytterbium concentrations in the first 18 samples range from 0.03 to 0.17 ppm (Yb_{PM} = 0.09–0.4). Such low Yb concentrations are usually the result of melting in the absence of garnet but cratonic garnet lherzolites with comparably low Yb contents and containing garnet with low abundances of HREE have been reported elsewhere (e.g. Pearson et al., 2003). Hence, the low Yb contents could be the result of complete garnet consumption by partial melting (with subsequent exsolution during cooling) or melting in the spinel stability field and subsequent incorporation deeper in the lithosphere (e.g. Kelemen et al., 1998; Wittig et al., 2008).

Abundances of large ion lithophile elements (e.g. Ba, Rb, Sr) and high field strength elements (e.g. Ti, Ta, Nb, Zr, Hf) are slightly to strongly enriched compared to the primitive mantle (Ba_{PM} = 7–351, Rb_{PM} = 13–67, Nb_{PM} = 3.6–39.5, Zr_{PM} = 0.4–4.4). The HFSE enrichments are interpreted as the result of lamproite infiltration of the xenoliths: this is supported by strong correlations amongst these elements (i.e. Ta vs. Hf (r = 0.96); Zr vs. Ti (r = 0.86)) tending toward the lamproite composition. Similarly, apart from one sample (6504256), rubidium varies sympathetically with strontium (r = 0.72) also tending toward the lamproite composition. The same is true for Sr and Rb variations as a function of Ba contents but only for 16 of the 24 samples. The 8 remaining samples show the highest Ba concentrations whose variations are independent of any other trace elements analysed here. These enrichments are not obviously linked to the lamproite infiltration. In addition to the clear evidence of lamproite infiltration, Jaques et al. (1990) suggested that at least some of the enrichment in incompatible elements of the Argyle peridotite xenoliths was 'primary' and occurred prior to entrainment in the lamproite because of the presence of rare coarse Cr-rich titanate with high abundances of K, Ca, Sr, Ba and Zr, and K-rich Cr-diopside. Moreover, the Sm–Nd (and Rb–Sr) systematics of the Argyle lamproite imply derivation from a mantle source(s) enriched prior to 2000 Ma (Jaques et al., 1989a). Other evidence for metasomatic enrichment of the mantle beneath the HCO is the presence of pyrope with elevated Ti (and Zr) in the Argyle heavy mineral concentrates (Fig. 2, C.B. Smith, unpubl. data) that imply melt metasomatism (Griffin et al., 1999).

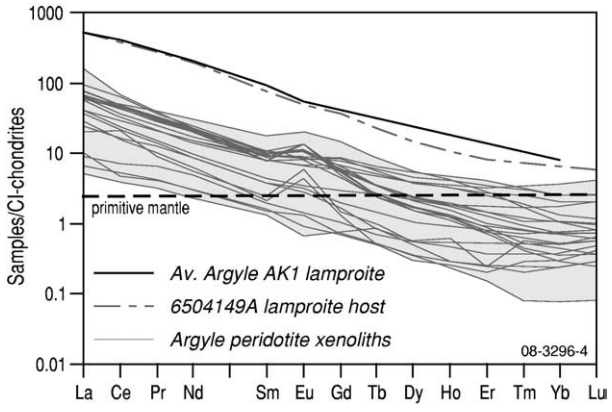

Fig. 4. Rare earth element (REE) abundances of the Argyle peridotite xenoliths normalized to CI-chondrites. Also shown are the REE contents of lamproite host sample 65041549A (this study) and the average Argyle AK lamproite (Jaques et al., 1989a). Note the marked depletion in HREE of the argyle peridotites and their strong enrichment in LREE, similar to that observed in the lamproite host.

7. Osmium, Rhenium and $^{187}Os/^{188}Os$ ratios

7.1. Replicate analyses

Whole-rock Re–Os analyses have been replicated for 8 samples (both diamondiferous and non-diamondiferous) by Carius tube and/or HP-asher digestions. Replicate analyses can yield information on the Os and Re-bearing mineral(s) in the Argyle mantle samples such as their distribution at the hand sample scale and the numbers of populations of host minerals.

Xenoliths N 23, 6504270, 6504142 and 6504131 yield similar Os and Re concentrations as well as similar Re–Os ages (Fig. 5) for digestions performed by the 2 different techniques and on different amounts of powder. The excellent reproducibility of the Os and Re concentrations and T_{RD} ages demonstrates that the Os-bearing minerals are homogeneously distributed at the scale of 1 g and it is likely that only one population of Os-bearing minerals occurs in those samples. This conclusion is also supported by the highly reproducible HSE patterns (Luguet et al., 2008) that yield very similar HSE abundances and inter-element fractionations independent of the digestion procedure.

Other samples show more variability in their replicate analyses by different techniques. The large variations of Os concentrations in samples 6504138 and 6504257 likely reflect the occurrence of irregularly distributed Os-rich minerals in some of the aliquots analysed. HSE patterns in these Os-rich samples are also associated with positive Ru anomalies (see Luguet et al., 2008), revealing that the Os–Ru-rich minerals are likely laurite (see Luguet et al., 2007; Lorand et al., 2008). It seems unlikely that inefficient attack of laurite grains by one of the digestion method used here can explain the abundance variations we observe. This is reinforced by the identical Re–Os model ages obtained for the xenolith 6504131, which would not result from preferential leaching of an Os-rich phase and indicate that the laurite grains, together with the other Os-host minerals, are dominated by a single generation.

Surprisingly, we obtained lower Os concentrations from samples 6504293 and 6504091 via the HP-asher digestions compared to the Carius tube digestions. Re values were also lower; however, the shapes of the HSE patterns are similar between the two types of digestions. This suggests that the lower Os and Re concentrations measured for the HP-asher digestions likely reflect nugget effects rather than variations in digestion inefficiency. Typically, where variable and inefficient leaching operates in the dissolution of HSE-rich rocks, it is the Carius Tube technique that yields the lower HSE abundances relative to HP-HT digestions (Meisel and Moser, 2004). We do not observe these systematics in any of our replicate data. The different T_{RD} eruption ages obtained for a given sample could be explained by the difference of Os/Re ratios without inferring the occurrence of several generations of Os-hosts having different T_{RD} eruption ages.

Since there are no systematic differences in Re–Os systematics as a function of digestion method, only the Carius tube digestion data, are

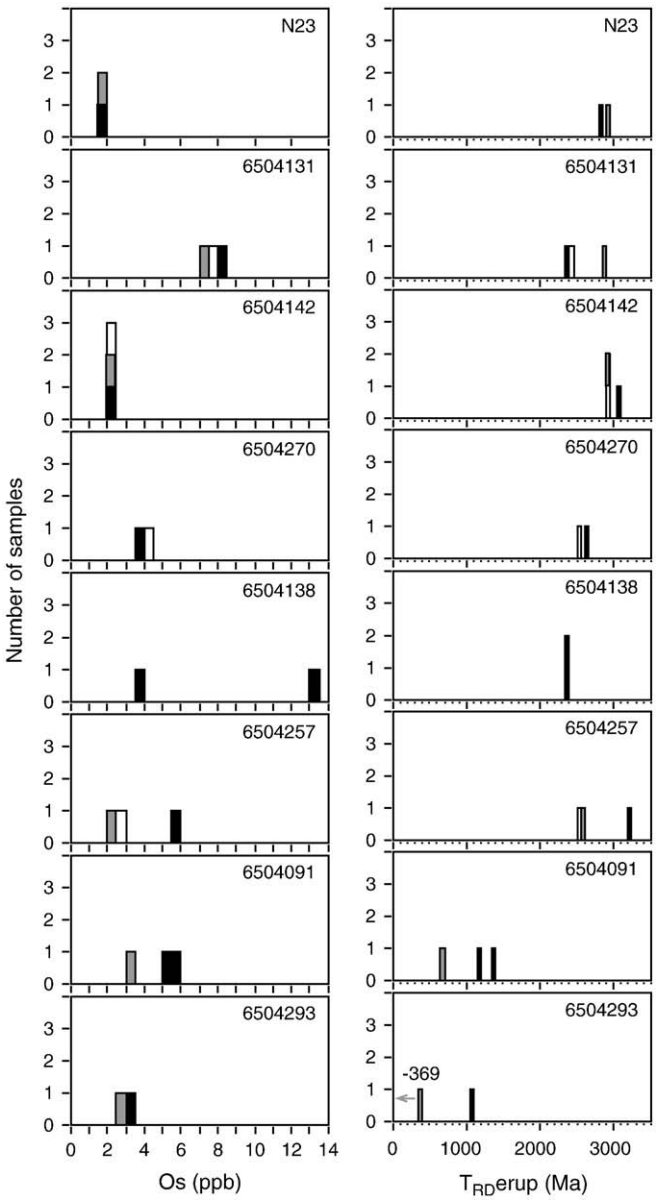

Fig. 5. Concentrations of osmium and T_{RD} eruption ages obtained for the replicate analyses of 8 Argyle sample xenoliths. The Os and Re analyses were performed on 1 g sample powder after Carius tube digestions (black symbol), on 1 g sample powder after HP-asher digestions (grey symbol) and on 2 g sample powder after HP-asher digestions.

used in the rest of this article for uniformity when discussing whole-rock Os and Re concentrations and Re–Os isotopic systematics.

7.2. Os and Re concentrations

The whole-rock Os and Re concentrations in the Argyle peridotite xenoliths lie in the range 1.67–13.34 ppb Os, 0.05–1.02 ppb Re (Table 2). There is no difference in the PGE abundances (or systematics) of diamondiferous and non-diamondiferous samples. These concentration ranges are similar to those reported for cratonic peridotites (Pearson et al., 2004) and overlap the concentration range found for off-craton xenoliths.

Mantle residues of high degrees of partial melting are expected to be strongly depleted in Re because of its highly incompatible behaviour (Reisberg and Lorand, 1995; Luguet et al., 2007). While Re/Os ratios of Argyle peridotites are mostly sub-chondritic (<0.08), they are much higher than expected for mantle samples having experienced extensive partial melting (~0.001-0.03). In addition, the HSE patterns of the Argyle samples (Luguet et al., in preparation; Luguet et al., 2008) show positively-sloped Pd-Re segments, i.e. the opposite trend to that expected for partial melting residues. These two features argue for post-melting Re enrichments in the Argyle peridotite xenoliths, most plausibly due to the lamproite infiltration. This melt infiltration may have also introduced some Os, leading to significant scattering of Re–Os isochron systematics and requiring the use of T_{RD} ages that assume all Re was removed at the time of melting and produce minimum ages.

Concentrations of Os and Re in the coarse primary chromite (fractions A and B) and isometric symplectite spinel (fractions C and D) separates are 0.29–53.39 ppb for Os and <0.015–1.34 ppb for Re. Apart from fraction C, osmium concentrations in the chromite and spinel separates are similar and fall in the same concentration interval than the one obtained on chromites from highly depleted harzburgites from Lherz (Luguet et al., 2007). On the other hand, the symplectite spinels have low Re contents, slightly lower than the Re contents from the sulfide-free Lherz

Table 2
Osmium and rhenium concentrations, 187Os/188Os ratios and TRD ages at the time of the eruption of the lamproite for the Argyle peridotite xenoliths.

Sample		Os ppb	Re ppb	$^{187}Os/^{188}Os$	$T_{RD\ erup}$
Whole-rock					
6504022		4.63	0.3	0.117961	2354
6504072		3.51	0.48	0.120627	2922
6504091		5.53[a]	0.50[a]	0.128866[a]	1183[a]
		5.28[a]	0.61[a]	0.130028[a]	1360[a]
		3.48[b]	0.53[b]	0.138642[b]	653[b]
6504093		4.31	0.11	0.116011	2115
6504096		4.85	0.05	0.118384	1582
6504111		3.96	0.17	0.112808	2776
6504131	◆	8.23[a]	1.02[a]	0.123504[a]	2369[a]
		7.46[b]	0.99[b]	0.120401[b]	2894[b]
		7.53[c]	0.87[c]	0.122227[c]	2426[c]
6504138		3.68[a]	0.85[a]	0.133705[a]	2378[a]
		13.34[a]	0.92[a]	0.118269[a]	2357[a]
6504142		2.21[a]	0.15[a]	0.112627[a]	3082[a]
		2.13[b]	0.12[b]	0.112929[b]	2901[b]
		2.26[c]	0.11[c]	0.112204[c]	2902[c]
6504148	◆	5.48	0.55	0.120491	2471
6504149	◆	1.72	0.05	0.113891	2467
6504158		3.41	0.16	0.113444	2736
6504180		3.41	0.16	0.118058	2247
6504221		6.88	0.15	0.113003	2467
6504256		3.93	0.19	0.117792	2146
6504257		5.88[a]	0.40[a]	0.111642[a]	3247[a]
		2.32[b]	0.05[b]	0.112072[b]	2577[b]
		2.89[c]	0.04[c]	0.111951[c]	2521[c]
6504270	◆	3.90[a]	0.13[a]	0.112908[a]	2610[a]
		4.15[c]	0.06[c]	0.111734[c]	2528[c]
6504271	◆	3.69	0.27	0.119284	2277
6504293		3.12[a]	0.55[a]	0.137919[a]	1085[a]
		2.50[b]	0.32[b]	0.143521[b]	369[b]
6504294		5.42	0.2	0.113518	2580
N23		1.67[a]	0.11[a]	0.114579[a]	2807[a]
		1.88[b]	0.12[b]	0.113490[b]	2946[b]
N25		1.76	0.05	0.111002	2792
N40	◆	5.7	0.28	0.116926	2301
N48		6.61	0.29	0.113933	2636
HR 6504149		0.82	0.14	0.130091	n.d.
Chromite Separates					
6504257-A		0.29[a]	1.34[a]	0.093440[a]	45013[a]
6504257-B		3.90[a]	0.87[a]	0.109922[a]	5416[a]
6504257-C[d]		53.39[b]	b.d.l.[b]	0.120277[b]	1184[b]
6504257-D		0.40[b]	0.033[b]	0.127449[b]	1263[b]

n.d.: not determined, b.d.l.: below detection limit. Diamond symbol stands for the diamondiferous xenoliths.
$^{187}Os/^{188}Os$ ratios and T_{RD} ages at the time of the eruption of the lamproite for the Argyle peridotite xenoliths.
[a] Carius-tube digestions (different weights for chromite separates, see text).
[b] HP-asher digestions on 1 g rock powder (different weights for chromite separates, see text).
[c] HP-asher digestions on 2 g rock powder.
[d] T_{RD} eruption calculated using a b.l.d concentration for Re of 15 ppt (i.e. 3 × Re blank).

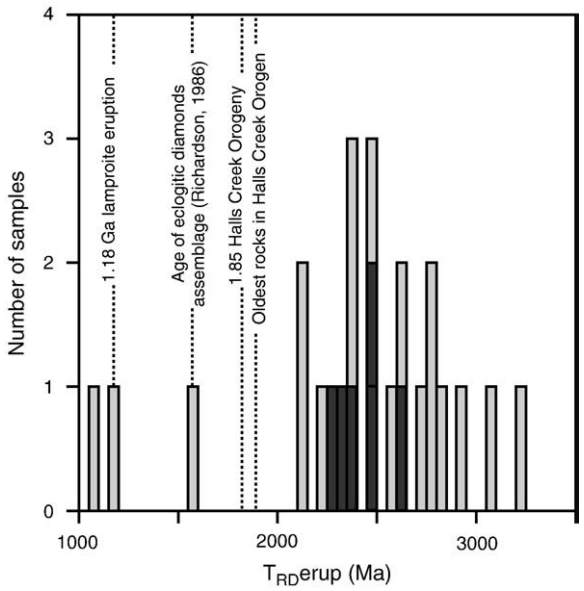

Fig. 6. Histogram of T_{RD} model ages for Argyle peridotite xenoliths (diamondiferous xenoliths in black, non diamondiferus xenoliths in grey) corrected for the age of eruption of the Argyle lamproite. Also indicated are the ages and age ranges of significant regional crustal events.

harzburgites (Luguet et al., 2007) whereas the primary chromites have high Re contents (as well as higher incompatible PGE contents, see Luguet et al., 2008), higher than the chromites from Lherz harzburgites. Consequently, the primary chromites are characterised by elevated Re/Os ratios (0.22–4.60) while the symplectite spinels show much lower Re/Os ratios (0.0002–0.08).

7.3. Re–Os ages

Because the Re abundances of the Argyle peridotite xenoliths are not primary, Re–Os model ages (T_{MA}) will overestimate the ages, as appears to be the case for two peridotites analyzed by Graham et al. (1999). As Re is most likely to have been introduced by the lamproite host, we have calculated T_{RD} eruption ages for the Argyle peridotite xenoliths assuming that the measured Re abundances were introduced to a Re-depleted mantle peridotite residual after partial melting (with Re/Os = 0) at the time of eruption of the Argyle lamproite (1180 Ma). The T_{RD} eruption ages calculated in this way are minimum ages if this assumption is true, and will produce ages that are older than the simple T_{RD} model ages that are calculated from present-day Os isotope compositions. Such T_{RD} eruption ages will always produce dates that are younger than whole rock T_{MA} ages, which will over-estimate the age of most metasomatised cratonic peridotites (see Pearson et al., 1995a, 2004 for a fuller explanation).

The Re–Os model (T_{RD} eruption) ages for the Argyle peridotite xenoliths range from 1.1 to 3.2 Ga with most yielding Paleoproterozoic to Neoarchean model ages of 2.2–2.9 Ga (Fig. 6). Xenoliths with the best preserved primary silicate assemblage all recorded T_{RD} eruption ages ≥ 2.3 Ga (2.3-2.9 Ga) whereas all T_{RD} eruption ages younger than 2.3 Ga came from samples with no primary silicates remaining. However, some older T_{RD} eruption ages were also obtained from a number of xenoliths with no primary silicates remaining. These model ages are in fact minimum ages and clearly establish an Archean age for at least some of the Argyle peridotite xenoliths. There is no discernable difference in model age systematics between diamondiferous and non-diamondiferous xenoliths. Nor is there any variation in model age with estimated equilibration pressure, which is perhaps not unexpected given the restricted depth range of xenolith sampling (Fig. 2).

Coarse 'primary' chromites from sample 6505247 yield unrealistic Re–Os model ages of >5.4 Ga, likely due to an ^{187}Re ingrowth over-correction imposed by their high Re/Os ratios. Symplectite spinel fractions yielded Re–Os T_{RD} eruption ages of 1184 Ma and 1263 Ma. (Table 2), close to the time of eruption of the Argyle lamproite (1180 Ma). This suggests that the alteration of the former garnet to form the symplectites may have occurred during incorporation of the xenoliths into the early-forming lamproite melt, or during its eruption to surface.

8. Discussion

8.1. Comparison with other Archean Cratons

The Argyle peridotite xenoliths share a number of features characteristic of Archean cratonic continental lithospheric mantle (CLM) inferred to be the residue of large degrees of partial melting. They have olivine compositions that span the range reported from many other Archean cratons. The average Argyle peridotite olivine (35 samples) of $Fo_{92.1 \pm 0.4}$ is within uncertainty of the pronounced mode for 'typical' Archean CLM of $Fo_{92.6}$ (Pearson and Wittig, 2008) but is more like that found in Neoarchean CLM (e.g. Somerset Island; Schmidberger and Francis, 1999; Irvine et al., 2003), which averages $Fo_{92.15}$. All are consistent with an origin as the residue from the partial melting of fertile mantle peridotite. In contrast, chrome pyrope garnets recovered from heavy mineral concentrates from the Argyle pipe are typically Ca-rich and low in Cr (G9 in Dawson and Stephens, 1975 classification scheme) indicating derivation from lherzolitic rather than harzburgitic CLM (Lucas et al., 1989): such compositions are thought more typical of Proterozoic or Neoarchean than older Archean CLM. However, as noted earlier, Jaques et al. (1989b) reported a Cr-rich, Ca-low (G10 in Dawson and Stephens, 1975 classification scheme) garnet inclusion from an Argyle peridotitic diamond and these inclusions are generally associated with typical Archean CLM.

Similarly, the low Al_2O_3, CaO and Na_2O contents, low abundances of Ti, Zr, Y, Sc and V, and high $Mg^{\#}$ of the Argyle peridotites are very similar to the depleted levels found in cratonic CLM. They are more refractory than those of Proterozoic and younger CLM as shown in the $Mg^{\#}$ versus Al_2O_3 variation plot (Fig. 7). In addition to having similar depletion trends to Archean cratonic mantle, the Argyle peridotites are also characterized by a specific SiO_2 vs MgO trend, which overlaps that of Archean cratonic mantle and some fore-arc peridotites (e.g. Izu Bonin). However, if the SiO_2 contents are taken as primary, the Argyle samples would be the most silica-rich cratonic mantle samples reported so far. The high SiO_2 contents could result from 1) extensive orthopyroxene replacement by talc, 2) incorporation of lamproite and /or country rocks within the xenolith, or 3) orthopyroxene enrichment as suggested for the Kaapvaal high-SiO_2 xenoliths (Kelemen et al., 1998; Simon et al., 2007). Variable SiO_2 feature seems widespread in cratonic peridotites as a whole (Pearson and Wittig, 2008), with some cratonic roots, e.g. Kaapvaal, having very elevated SiO_2 while others, e.g., Greenland, have much lower SiO_2 contents. The process generating the variations in SiO_2 seems to be related to the formation and/or modification of continental sub-lithospheric mantle generally.

The Re–Os T_{RD} eruption model ages of the Argyle peridotite xenoliths overlap the range found for kimberlite-borne peridotite xenoliths from other cratons from Southern Africa (Pearson et al., 1995a; Carlson et al., 2005), Northern Canada (Irvine et al., 2003; Westerlund et al., 2006), Siberia (Pearson et al., 1995b), Greenland (Bernstein et al., 2006; Pearson and Wittig, 2008) and Tanzania (Chesley et al., 1999) (Fig. 8). CLM sampled by off-craton kimberlites typically have Proterozoic or younger Re–Os model ages (Fig. 8; Pearson, 1999; Carlson et al., 2005).

8.2. Lithospheric root to the Kimberley Craton

The P–T estimates coupled with the Re–Os T_{RD} eruption model ages demonstrate the existence of Archean lithosphere stabilised within the field of diamond formation at depths of 160–190 km beneath the Argyle pipe in the HCO. The late Archean Hf model ages reported by Downes

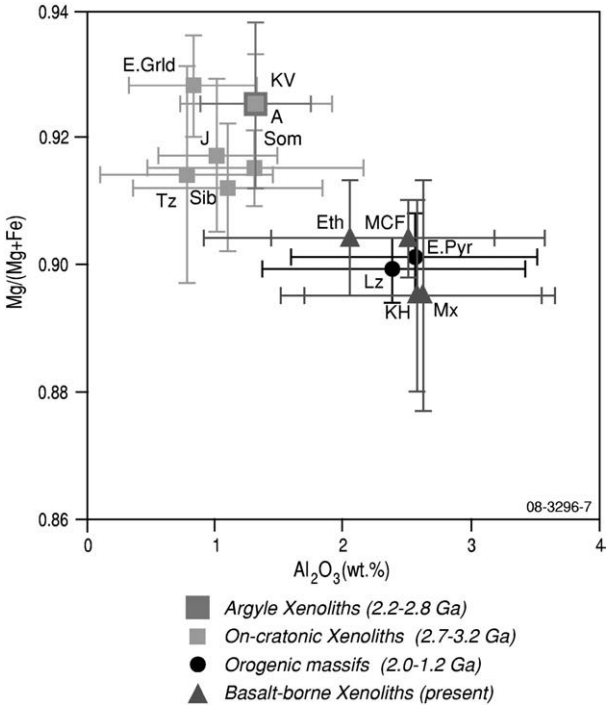

Fig. 7. Mg/(Mg+Fe) versus Al_2O_3 for Argyle peridotite xenoliths (A) compared with xenoliths from on-craton kimberlites, xenoliths from off-craton basalts and orogenic massifs. Data for on-craton xenoliths are from Kaapvaal (KV: Boyd and Mertzman, 1987), from Tanzania (Tz: Rudnick et al., 1993, 1994; Lee and Rudnick, 1999), from Siberia (Sib: Boyd et al, 1997), from Jericho (J: Kopylova and Russell, 2000), from Somerset (Som: Irvine et al., 2003), East Greenland (E. Grld: Bernstein et al, 1998). Data for the orogenic massifs are from East Pyrenees (Bodinier et al, 1988; Fabries et al., 1989, 1998; Reisberg and Lorand, 1995) and Lanzo (Bodinier, 1988; Bodinier et al., 1991). Data for the basalt-borne xenoliths are from French Massif Central (MCF: Zangana et al., 1999), from Ethiopia (Eth: Bedini et al., 1997), from West Mexico (Mx: Luhr and Aranda-Gomez, 1997) and from the Kilbourne Hole (Jagoutz, 1979).

et al. (2007) for Paleoproterozoic (1850 Ma, U–Pb method) zircons in peridotite xenoliths from the Aries kimberlite suggest that Archean lithosphere may extend beneath the Kimberley Craton. The presence of sub-calcic Cr-pyrope (harzburgitic) garnets in concentrate from kimberlites in the North Kimberley province implies the survival of Archean lithosphere beneath that region although lherzolitic garnets predominate and define a conductive model geotherm of 40 mW/m^2 (O'Reilly et al., 1997). Similarly, the nitrogen-aggregation characteristics (Taylor et al., 1990) and the low $^{187}Os/^{188}Os$ initial ratio of sulfide inclusions in Ellendale diamonds (Smit et al., 2008; this volume) suggest that Archean lithosphere may extend to the southern margin of the Kimberley Craton. Present day S-wave seismic tomography indicates thick lithosphere extending to 225-250 km depth beneath the Kimberley Craton (Van Der Hilst et al., 1998; Fishwick et al., 2005). The Re–Os data, coupled with the seismic tomography, implies the survival of an Archean diamondiferous lithospheric root beneath the Kimberley Craton from at least the time of lamproite eruption to the present day.

Whole rock Re–Os T_{RD} eruption ages are almost certainly minima given the multi-stage HSE evolution indicated by the Argyle xenolith bulk rock HSE patterns (Luguet et al., in preparation; Luguet et al., 2008). None-the-less, these T_{RD} eruption ages show that the lithosphere beneath the HCO, a Paleoproterozoic orogenic belt, is at least Neoarchean in age, even at depths of 150–200 km. The Re–Os model ages are significantly older than the oldest crustal rocks in the HCO (~1920 Ma) and thus suggest that the crust and mantle beneath the HCO have been decoupled. The nearest outcrops of basement of late Archean (2600–2500 Ma) age lie more than 400 km further east in the Pine Creek Inlier (Worden et al., 2008) and in the Billabong complex within the Granites–Tanami region (Page et al., 1995). Detrital zircons of late Archean (and older) ages are widespread in Proterozoic sedimentary and metasedimentary sequences across the North Australian Craton but their provenance is uncertain (Tyler et al., 1999; Hoatson and Blake, 2000). Despite substantial thermal reworking and formation of new crust at ~1860-1800 Ma (Hoatson and Blake, 2000; Griffin et al., 2000; Betts et al., 2002) the amalgamation of these different tectonic blocks did not eliminate Archean CLM underpinning the region.

8.3. The nature of the lithospheric root and origin of Argyle peridotitic diamonds

Although the Argyle peridotitic xenoliths appear to have been derived from a relatively restricted PT range and show no significant variation in bulk chemistry (major or trace elements) or Re–Os age over this depth range, combining our data, earlier data from the peridotitic xenoliths, diamonds and their inclusions (Sobolev et al., 1989; Jaques et al., 1989b) with information from pyrope and chromite

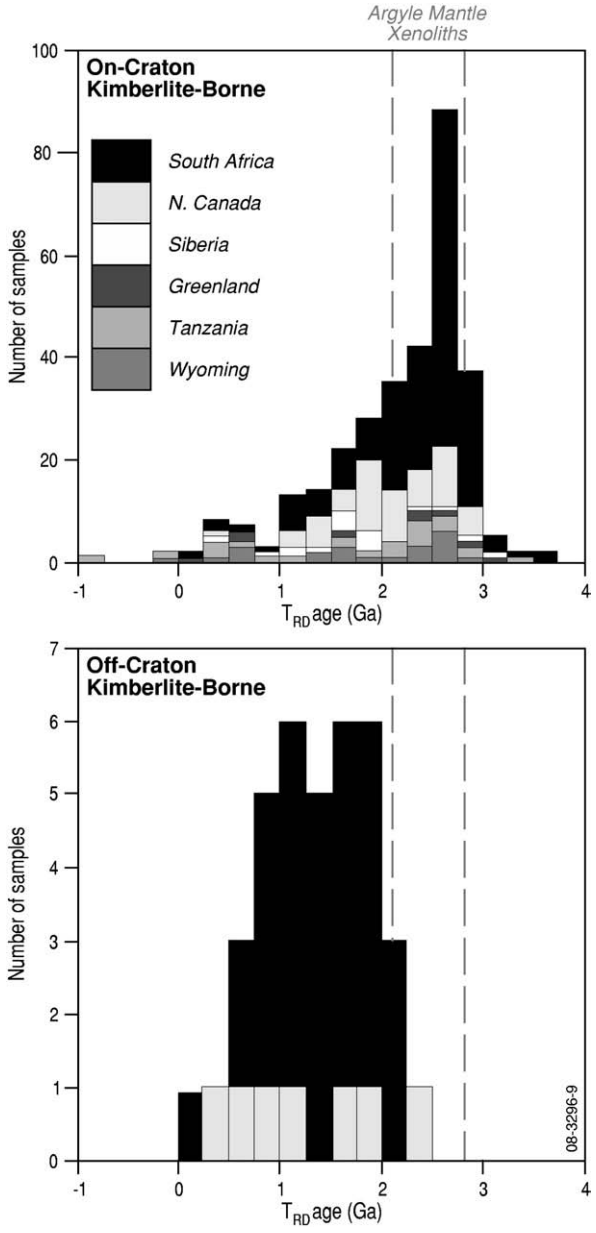

Fig. 8. Histogram comparison of T_{RD} ages between cratonic and circum-cratonic ("off-craton") kimberlite-hosted peridotite xenoliths with the range for the least disturbed Argyle samples shown. Data sources are those given in Pearson et al. (2004) and Carlson et al. (2005).

macrocrysts from the lamproite concentrate, gives a more complete picture of the chemistry and depth of the mantle sampled by the Argyle pipe.

The first source of information comes from diamonds and their inclusions. The microdiamonds from peridotitic xenoliths match in all their properties, such as octahedral morphology, colour, N aggregation, chemistry of olivine inclusions and carbon isotope values corresponding to a mantle signature of −5 to −6‰, with a population of small peridotitic diamonds from the Argyle lamproite commercial production (Hall and Smith, 1984; Jaques et al, 1986). The similarity in chemistry of xenolith olivines and the olivine inclusion in a xenolith diamond indicate that the microdiamonds have a primary nature in these peridotites. It can be concluded that the diamonds were formed in peridotitic mantle rocks at the same PT and time as the other xenolith minerals. It follows therefore that the microdiamonds are much older (~2.3–2.6 Ga) than the commercial size eclogitic stones which are believed to have formed at ~1.58 Ga, based on Sm–Nd dating of garnet and clinopyroxene inclusions (Richardson, 1986). The heavy carbon isotope composition of the small peridotitic diamonds implies their formation in the mantle under reduced conditions without input of subducted material, most likely from methane, as proposed by Jaques et al (1989b).

The second source of information about mantle source sampled by the lamproite is mineral concentrate. Thus concentrate-derived chrome pyrope garnets from the Argyle lamproite are predominately lherzolitic with an essentially depleted trace element signature (i.e. low Zr, Y, Ti), suggesting a depleted lherzolitic rather than harzburgitic CLM beneath the HCO. The sole harzburgitic pyrope found as a diamond inclusion (Jaques et al., 1989b) has a similar depleted trace element composition. However, a minor portion of the Argyle concentrate chrome pyrope garnets show enhancements in Ti and commonly Zr and Y (C.B. Smith, unpubl. data, Fig. 2), characteristic of mantle affected by melt metasomatism (Griffin et al., 1999). Thermobarometric calculations using the Ni-in-garnet thermometer (Canil, 1999) and Cr-in garnet barometers (Ryan et al., 1996) place most of the lherzolite garnets in the graphite stability field with the Ti-melt metasomatised garnets extending slightly deeper toward the PT field of the Argyle peridotite xenoliths (Fig. 2). This melt metasomatism event in the lithosphere may be the agent for the metasomatic enrichment of the Argyle peridotite xenoliths reported by Jaques et al. (1990) and may have disrupted some of the Re–Os systematics within the peridotite xenoliths. The presence of a low-Ca harzburgitic pyrope diamond inclusion at Argyle may reflect a remnant earlier lithology that survived the melt metasomatism by being encapsulated in the diamond.

The Argyle eclogitic diamonds that form the bulk of the commercial-sized diamonds are estimated to have formed at similar or greater mantle depths to the peridotitic xenoliths analysed here. Jaques et al. (1989b) and Sobolev et al. (1989) reported equilibration temperatures for inclusions in Argyle eclogitic diamonds in the range 1140–1350 °C (average ~1245 °C). The Simakov (2008) eclogite thermobarometer (aluminium solubility in clinopyroxene coexisting with garnet) yields equilibration conditions of 6–7.2 GPa and 1250–1350 °C that compare with pressures of 6–6.5 GPa estimated from K solubility in diopside (Safonov et al., 2008). These constraints place the Argyle eclogitic diamonds at depths of 200–225 km corresponding to base of the present day lithosphere beneath the HCO based on seismic S-wave tomography (Fishwick et al., 2005).

8.4. Formation of the lithospheric root

The T_{RD} ages of the Argyle peridotite xenoliths do not correlate with any known crustal rocks or events in the Kimberley Craton. Significantly, the Re–Os systematics of the Argyle peridotites do not record the major thermal events associated with mafic (1860–1830 Ma, 1790 Ma) and felsic magmatism (1910, 1880–1790 Ma) or orogenesis (~1865–1835 Ma; Hoatson and Blake, 2000; Bodorkos et al., 2000) in the HCO. Nor is the 1.58 Ga age of formation of the eclogitic suite diamonds reflected in the peridotite Re–Os data. The age of the Argyle eclogitic diamonds coincides with major 1.60–1.58 Ga thermal and tectonic (crustal shortening) events at the southern (Chewings Orogeny) and eastern (Isan orogeny) margins of the North Australian Craton and the southeast (Hiltaba Event, Olarian Orogeny) Proterozoic terranes of the South Australian craton (e.g. Betts et al., 2002; Giles et al., 2004; Betts and Giles, 2006). This coincidence of eclogitic diamond formation and widespread tectonothermal events affecting many of the Proterozoic terranes suggests a link with subduction-accretion processes that added Mesoproterozoic diamonds to the diamondiferous late Archean root zones beneath the HCO. Jaques et al. (1989b) suggested on the basis of the inclusion assemblage and their distinct carbon isotopic compositions ($\delta^{13}C$ typically −9 to −12‰) that the Argyle eclogitic diamonds formed in subducted oceanic crust that was accreted to the base of the lithosphere in the Proterozoic. This is perhaps analogous to the proposed link between eclogitic diamond formation and the craton evolution proposed elsewhere (Shirey et al., 2003, 2004).

9. Conclusion

Our study provides definitive evidence that the Argyle diamond pipe is underlain by (Neo)-Archean lithospheric mantle (2.1–3.2 Ga) based on Re–Os dating of peridotite xenoliths derived from within the diamond stability field near the base of the lithosphere (160–190 km depth). This thick (200–225 km) diamondiferous lithosphere is imaged by present day seismic S-wave tomography. The peridotites are of lherzolite composition and not as refractory as those found beneath many older Archean cratons. They have mineral and bulk rock compositions that are consistent with an origin as residues of partial melting of primitive mantle peridotite. The origin of the peridotite is uncertain but the low abundances of HREE suggest they may have formed initially within the spinel peridotite stability field and have been subducted to their present depths, in line with most other cratons (Canil, 2004; Wittig et al., 2008; Pearson and Wittig, 2008). Alternatively, partial melting may have occurred in the garnet stability field until the consumption of garnet. However, as garnet is stable in melting residues to very high degrees of melting (Walter, 2003), we prefer a shallow melting origin. The existence of lithosphere of late Archean age beneath the Argyle diamond pipe, even though no crustal rocks of Archean age are known from the region, suggests a decoupling of the crust and mantle in the region of the HCO, perhaps as a consequence of Paleoproterozoic (~1.85 Ga) reworking of and/or subduction at the margin of the Kimberley Craton. The confirmation of an Archean lithospheric root beneath the Argyle pipe at the margin of the Kimberley Craton seemingly conforms with the restriction of economic diamond deposits to those underlain by Archean lithosphere.

The xenolith microdiamonds have a spotty and erratic distribution: many xenoliths are barren of diamond; others carry minor to extremely high diamond grade. The microdiamonds recovered from Argyle peridotite xenoliths have unresorbed octahedral shapes and correspond in properties with a small population of peridotitic octahedral diamonds occurring in the commercial production from the lamproite. However, Argyle owes its rich diamond grades not to its Neoarchean mantle root but to Proterozoic accretion of richly diamondiferous eclogitic material to the craton root.

Acknowledgements

We thank Argyle Diamonds and Rio Tinto Ltd for logistical assistance and the staff of the Argyle mine and Grant Boxer for recovery of the xenoliths. The chromite separates were prepared by Lauren Jackson and Tas Armstrong (GA), and by Z. Martelli (Rio Tinto) who also arranged for recovery of diamonds from the xenoliths. Chris Ottley (DU) assisted with PGE method development on the Element 2. AL thanks the European Union for the Marie Curie Post-doctoral Fellowship (EIF-ENV-009752) during which this study was

performed. Reviews by Sonia Aulbach and another conference reviewer assisted the presentation and clarity of the manuscript. ALJ publishes with the permission of the CEO, Geoscience Australia.

Appendix A. Supplementary data

Supplementary data associated with this article can be found, in the online version, at doi:10.1016/j.lithos.2009.05.022.

References

Bedini, R.M., Bodinier, J.-L., Dautria, J.-M., Morten, L., 1997. Evolution of LILE-enriched small melt fractions in the lithospheric mantle: a case study from the East African Rift. Earth and Planetary Science Letters 153, 67–83.

Bernstein, S., Kelemen, P.B., Brooks, C.K., 1998. Depleted spinel harzburgite xenoliths in Tertiary dykes from East Greenland: Restites from high melting degrees. Earth and Planetary Science Letters 154, 221–235.

Bernstein, S., Hanghøj, K., Kelemen, P.B., Brooks, C.K., 2006. Ultra-depleted, shallow cratonic mantle beneath West Greenland: dunitic xenoliths from Ubekendt Ejland. Contributions to Mineralogy and Petrology 152, 335–347.

Betts, P.G., Giles, D., 2006. The 1800 Ma to 1100 Ma tectonic evolution of Australian. Precambrian Research 144, 92–125.

Betts, P.G., Giles, D., Lister, G.S., Frick, L.R., 2002. Evolution of the Australian lithosphere. Australian Journal of Earth Sciences 49, 661–695.

Bodinier, J.-L., 1988. Geochemistry and petrogenesis of the Lanzo peridotite body, western Alps. Tectonophysics 149, 67–88.

Bodinier, J.-L., Dupuy, C., Dostal, J., 1988. Geochemistry and petrogenesis of eastern Pyrenean peridotites. Geochimica et Cosmochimica Acta 52, 2893–2907.

Bodinier, J.-L., Menzies, M.A., Thirlwall, M., 1991. Continental to ocanic mantle transition—REE and Sr–Nd isotopic geochemistry of the Lanzo lherzolite massif. Journal of Petrology (Orogenic lherzolites and mantle processes 191–210 special volume.

Bodorkos, S., Cawood, P.A., Oliver, N.H.S., Nemchin, A.A., 2000. Rapidity of orogenesis in the Paleoproterozoic Halls Creek Orogen, northern Australia: Evidence from SHRIMP zircon data, CL zircon images and mixture modeling studies. American Journal of Science 300, 60–82.

Boxer, G.L., Lorenz, V., Smith, C.B., 1989. The geology and the volcanology of the Argyle (AK1) lamproite diatreme, Western Australia. In: Ross, J., et al. (Ed.), Kimberlites and Related Rocks, Vol. 1, Their Composition, Occurrence, Origin and Emplacement: Geological Society of Australia Special Publication, Vol. 14, pp. 140–152.

Boyd, F.R., Mertzman, S.A., 1987. Composition and structure of the Kaapvaal lithosphere, Southern Africa. In: Mysen, B.O. (Ed.), In magmatic processes: Physicochemical principles: The Geochemical Society, Houston, vol. 1, pp. 3–12.

Boyd, F.R., Pokhilenko, N.P., Pearson, D.G., Mertzman, A.S., Sobolev, N.V., Finger, L.W., 1997. Composition of the Siberian cratonic mantle: evidence from Udachnaya peridotite xenoliths. Contributions to Mineralogy and Petrology 128, 228–246.

Brey, G.P., Kohler, T., 1990. Geothermobarometry in four phase lherzolites II: New thermobarometers and practical assessment of using thermo-barometers. Journal of Petrology 31, 1353–1378.

Bulanova, G.P., Smith, C.B., Kohn, S.C., Walter, M.J., Gobbo, L., Kearns, S., 2008a. Machado River, Brazil – a newly recognised ultradeep diamond occurrence. 3 pp.

Bulanova, G.P., Smith, C.B., Walter, M.J., Blundy, J., Gobbo, L., EIMF, Kohn, S.C., 2008b. Proto-kimberlitic ultra-deep diamonds from Collier 4 kimberlite pipe, Juina, Brazil. 9th International Kimberlite Conference Extended Abstract No. 9IKC-A-00227. 3 pp.

Canil, D., 1999. The Ni-in-Garnet geothermometer; calibration at natural abundances. Contributions to Mineralogy and Petrology 136, 240–246.

Canil, D., 2004. Mildly incompatible elements in peridotites ad the origin of mantle lithosphere. Lithos 77, 375–393.

Carlson, S.M., Hillier, W.D., Hood, C.T., Pryde, R.P., Skelton, D.N., 1999. The Buffalo Hills kimberlites: a newly discovered diamondiferous kimberlite province in north-central Alberta, Canada. Proceedings of the 7th Int. Kimberlite Conference, Volume 1, pp. 109–116.

Carlson, R.W., Pearson, D.G., James, D.E., 2005. Physical, chemical and chronological characteristics of continental mantle. Reviews in Geophysics 43, RG1001. doi:10.1029/2004RG000156.

Chesley, J.T., Rudnick, R.L., Lee, C.T., 1999. Re–Os systematics of mantle xenoliths from the east African rift: age, structure and history of the Tanzanian craton. Geochimica et Cosmochimica Acta 63, 1203–1217.

Dawson, J.B., Stephens, W.E., 1975. Statistical classification of garnets from kimberlite and associated xenoliths. Journal of Geology 83, 589–607.

Deines, P., 2002. The carbon isotope geochemistry of mantle xenoliths. Earth-Science Reviews 58 (3–4), 247–278.

Denny, M.B., 1998. Major and trace element discrimination of chromian spinels with particular application to the provenance of diamond indicator chromite from the Yilgarn craton, Western Australia. Unpublished Honours thesis, Research School of Earth Sciences and the Department of Geology, The Australian National University, Canberra.

Downes, P.J., Griffin, B.J., Griffin, W.L., 2007. Mineral chemistry and zircon geochronology of xenocrysts and altered mantle and crustal xenoliths from the Aries micaceous kimberlite: Constraints on the composition and age of the central Kimberley Craton, Western Australia. Lithos 93, 175–198.

Etheridge, M.A., Rutland, R.W.R., Wyborn, L.A.I., 1987. Orogenesis and tectonic process in the Early to Middle Proterozoic of northern Australia. In: Kröner, A. (Ed.), Proterozoic Lithospheric Evolution: American Geophysical Union Geodynamics Series, vol. 17, pp. 131–147.

Evans, T., Harris, J.W., 1989. Nitrogen aggregation, inclusion equilibration temperatures and the age of diamonds. Kimberlites and Related Rocks, Volume 2, Their Mantle/Crust Setting, Diamonds and Diamond Exploration: In: Ross, J., et al. (Ed.), Geological Society of Australia Special Publication, Vol. 14, pp. 1001–1006.

Fabries, J., Bodinier, J.-L., Dupuy, C., Lorand, J.-P., Benkerrou, C., 1989. Evidence for modal metasomatism in the orogenic spinel lherzolite body from Caussou (northeastern Pyrenees, France). Journal of Petrology 30, 199–228.

Fabries, J., Lorand, J.-P., Guiraud, M., 1998. Petrogenesis of the amphibole-rich veins from the Lherz orogenic lherzolite massif (Eastern Pyrenees, France): a case study for the origin of orthopyroxene-bearing amphibole pyroxenites in the lithospheric mantle. Contributions to Mineralogy and Petrology 140 (4), 383–403.

Fishwick, S., Kennett, B.N.L, Reading, A.M., 2005. Contrasts in lithospheric structure within the Australian craton-insights from surface wave tomography. Earth and Planetary Science Letters 231, 163–176.

Giles, D., Betts, P.G., Lister, G.S., 2004. 1.8–1.5 Ga links between the North and South Australian Cratons and the Palaeo- to Mesoproterozoic configuration of Australia. Tectonophysics 380, 27–41.

Graham, S., Lambert, D.D., Shee, S.R., Smith, C.B., Reeves, S., 1999. Re–Os isotopic evidence for Archean lithospheric mantle beneath the Kimberly Bock, Western Australia. Geology 27, 431–434.

Griffin, W.L., Shee, S.R., Ryan, C.G., Win, T.T., Wyatt, B.A., 1999. Harzburgite to lherzolite and back again: metasomatic processes in ultramafic xenoliths from the Wesselton kimberlite, Kimberley, South Africa. Contributions to Mineralogy and Petrology 134, 232–250.

Griffin, T.J., Page, R.W., Sheppard, S., Tyler, I.M., 2000. Tectonic implications of Paleoproterozoic post-collisional high-K felsic igneous rocks from the Kimberley region of Northwestern Australia. Precambrian Research 101, 1–13.

Grütter, H., Latti, D., Menzies, A., 2006. Cr-saturation arrays in concentrate garnet compositions from kimberlite and their use in mantle barometry. Journal of Petrology 47, 801–820.

Hall, A.E., Smith, C.B., 1984. Lamproite diamonds- are they different? In: Glover, J.E., Harris, P.G. (Eds.), Kimberlite Occurrence and Origin: A Basis for Conceptual Models in Exploration, Publication No 8. InThe Geology Department and University Extension, The University of Western Australia, Perth, pp. 167–212.

Hancock, S.L., Rutland, R.W.R., 1984. Tectonics of an early Proterozoic geosuture: The Halls Creek orogenic sub-province, Northern Australia. Journal of Geodynamics 1, 387–432.

Helmstaedt, H., 2009-this issue. Crust–mantle coupling revisited: The Archean Slave craton, NWT, Canada. Proceedings of the 9th International Kimberlite Conference. Lithos 112S, 1055–1068.

Hoatson, D.M., Blake, D.H., 2000. Geology and economic potential of the Palaeoproterozoic layered mafic-ultramafic intrusions in the East Kimberley, Western Australia. Canberra: Australian Geological Survey Organisation Bulletin 246 476 pp.

Irvine, G.J., Pearson, D.G., Kjarsgaard, B.A., Carlson, R.W., Kopylova, M.G., Breibus, G., 2003. A Re–Os isotope and PGE study of kimberlite-derived peridotite xenoliths from Somerset Island and a comparison to the Slave and Kaapvaal cratons. Lithos 71, 461–488.

Jagoutz, E., 1979. The abundances of major, minor and trace elements in the Earth's mantle as derived from ultramafic nodules. Proc. 10th Lunar Planetary Science Conference, pp. 2031–2050.

Janse, A.J.A., 1994. Is the Clifford's Rule still valid? Affirmative examples from around the world. In: Meyer, H.O.A., Leonardos, O.H. (Eds.), Diamonds: Characterisation, Genesis and Exploration, Proceedings from the 5th International Kimberlite Conference. InBrazil Companhia de Pesquisa de Recursos Minerais, Brazil, pp. 213–235.

Jaques, A.L., Milligan, P.R., 2004. Patterns and controls on the distribution of diamondiferous intrusions in Australia. Lithos 77, 783–802.

Jaques, A.L., Lewis, J.D., Smith, C.B., 1986. The kimberlites and lamproites from Western Australia. Geological Survey of Western Australia Bulletin 132 268 pp.

Jaques, A.L., Haggerty, S.E., Lucas, H., Boxer, G.L., 1989a. Geochemistry of the Argyle (AK1) lamproite pipe, Western Australia. Kimberlites and Related Rocks, Vol. 1, Their Composition, Occurrence, Origin and Emplacement: In: Ross, J., et al. (Ed.), Geological Society of Australia Special Publication, vol. 14, pp. 171–188.

Jaques, A.L., Hall, A.E., Sheraton, J.V., Smith, C.B., Sun, S.S., Drew, R., Foudoulis, C., Ellingsen, K., 1989b. Composition of crystalline inclusions and C-isotopic composition of Argyle and Ellendale diamonds. In: Ross, J., et al. (Ed.), Kimberlites and Related Rocks: Their Crust/Mantle Setting, Diamonds and Diamond Exploration. Geological Society of Australia Special Publication No14, vol. 2, pp. 966–989.

Jaques, A.L., O'Neill, H.St.C., Smith, C.B., Moon, J., Chappell, B.W., 1990. Diamondiferous peridotite xenoliths from the Argyle (AK1) lamproite pipe, Western Australia. Contributions to Mineralogy and Petrology 104, 255–276.

Kelemen, P.B., Hart, S.R., Bernstein, S., 1998. Silica enrichment in the continental upper mantle via melt/rock reaction. Earth and Planetary Science Letters 164, 387–406.

Kennett, B.L.N., 2003. Seismic structure in the mantle beneath Australia. In: Hills, R.R., Mueller, R.D. (Eds), Evolution and Dynamics of the Australian Plate, Geological Society of America 372; Geological Society of Australia, Special Publication 22, 7-23.

Klein, F., Bach, W., 2009. Fe–Ni–Co–O–S Phase relations in peridotite-seawater interactions. Journal of Petrology 50, 37–59.

Kopylova, M.G., Russell, J.K., 2000. Chemical stratification of cratonic lithosphere: constraints from the Northern Slave Craton. Earth Planetary Science Letters 181, 71–87.

Lambert, D.D., Shirey, S.B., Bergman, S.C., 1995. Proterozoic lithospheric mantle source for the Prairie Creek lamproites: Re–Os and Sm–Nd isotopic evidence. Geology 23, 273–276.

Lee, C.-T., 2002. Platinum-group element geochemistry of peridotite xenoliths from the Sierra Nevada and the Basin and Range, California. Geochimica et Cosmochimica Acta 66, 3005–3987.
Lee, C.-T., Rudnick, R.L., 1999. Compositionally stratified cratonic lithosphere: Petrology and geochemistry of peridotite xenoliths from the Labait tuff cone, Tanzania. In: Gurney, J.J., Gurney, J.L., Pascoe, M.D., Richardson, S.R. (Eds.), Proceedings of the 8th International Kimberlite Conference, J.B. Dawson volume, pp. 503–521.
Lorand, J.P., Pattou, L., Gros, M., 1999. Fractionation of platinum group element in the upper mantle: a detailed study in Pyrenean orogenic lherzolites. Journal of Petrology 40, 957–981.
Lorand, J.-P., Luguet, A., Alard, O., Bezos, A., Meisel, T., 2008. Abundance and distribution of platinum-group elements in orogenic lherzolites; a case study in a Fontete Rouge lherzolites, (French Pyrénées). Chemical Geology 248, 174–194.
Lucas, H., Ramsay, R.R., Hall, A.E., Smith, C.B., Sobolev, N.V., 1989. Garnets from Western Australia kimberlites and related rocks. In: Ross, J., et al. (Ed.), kimberlites and related rocks: Their Crust/Mantle Setting, Diamonds and Diamond Exploration. Geological Society of Australia Special Publication No14, vol. 2, pp. 809–819.
Luguet, A., 2000. Petrologie des sulfures de Fe-Ni-Cu et Geochimie des elements fortement siderophiles: Etude couplee dans les peridotites abyssales de la zone de fracture Kane (Zone Mark, 20-24°N, ride medio-atlantique) et de la campagne Edul (49-70°E, ride sud-ouest Indienne). Unpublished. Ph.D. thesis, Museum National d'Histoire Naturelle, Paris, France, 275 pp.
Luguet, A., Shirey, S.B., Lorand, J.-P., Horan, M.F., Carlson, R.W., 2007. Residual platinum-group minerals from highly depleted harzburgites of the Lherz massif (France) and their role in HSE fractionation of the mantle. Geochimica et Cosmochimica Acta 71, 3082–3097.
Luguet, A., Pearson, D.G., Jaques, A.L., Smith, C.B., Bulanova, G., Carter, G., Roffey, S., Rayner, M.J, Lorand, J.-P., 2008. Age constraints on the lithosphere beneath the Halls Creek mobile belt and implications for diamonds of the Argyle lamproite deposit. 9th International Kimberlite Conference Extended Abstract No. 9IKC-A-00263.
Luguet, A., Pearson, D.G., Jaques, A.L., Smith, C.B., Bulanova, G., Carter, G., Roffey, S., Rayner, M.J, Lorand, J.-P., in preparation. Evolution of the lithospheric root of the Kimberley Craton (Western Australia): Insights from HSE systematics of the peridotite xenoliths from the Argyle lamproite.
Luhr, J.F., Aranda-Gomez, J.J., 1997. Mexican peridotite xenoliths and tectonic terranes: Correlations among vent, location, texture, temperature, pressure, and oxygen fugacity. Journal of Petrology 38, 1075–1112.
McDonough, W.F., Sun, S.S., 1995. The composition of the Earth. Chemical Geology 120, 223–253.
Meisel, T., Moser, J., 2004. Reference materials for geochemical PGE analysis: new analytical data for Re, Rh, Pd, Os, Ir, Pt and Re by isotope dilution ICP-MS in 11 geological reference materials. Chemical Geology 208, 319–338.
Myers, J.S., Shaw, R.D., Tyler, I.M., 1996. Tectonic evolution of Proterozoic Australia. Tectonics 15 (6), 1431–1446.
Nimis, P., Taylor, W., 2000. Single clinopyroxene thermobarometry for garnet peridotites. Part I. Calibration and testing of a Cr-in-Cpx barometer and an enstatite-in-Cpx thermometer. Contributions to Mineralogy and Petrology 139 (5), 541–554.
O'Neill, H.St.C., Wood, B.J., 1979. An experimental study of Fe-Mg partitioning between garnet and olivine and its calibration as a geothermometer. Contributions to Mineralogy and Petrology 70, 59–70.
O'Reilly, S.Y., Griffin, W.L., Gaul, O., 1997. Paleo-geothermal gradients in Australia: key to 4-D lithosphere mapping. AGSO Journal of Australian Geology and Geophysics 17, 63–72.
Page, R.W., Sun, S.S., Blake, D., Edgecombe, D., Pearcey, D., 1995. Geochronology of an exposed late Archean basement terrane in the Granites-Tamani Region. AGSO Research Newsletter 22, 19–20.
Pearson, D.G., 1999. The age of continental roots. Lithos 48, 171–194.
Pearson, D.G., Wittig, N., 2008. Formation of Archaean continental lithosphere and its diamonds: the root of the problem. Journal of the Geological Society (London) 165, 1–20.
Pearson, D.G., Woodland, S.J., 2000. Solvent extraction/anion exchange separation and determination of PGEs Os, Ir, Pt, Pd, Ru and Re – Os isotopes in geological samples by isotope dilution ICP-MS. Chemical Geology 165, 87–107.
Pearson, D.G., Carlson, R.W., Shirey, S.B., Boyd, F.R., Nixon, P.H., 1995a. Stabilisation of Archean lithospheric mantle: A Re – Os isotope study of peridotite xenoliths from the Kaapvaal Craton. Earth and Planetary Science Letters 134, 341–357.
Pearson, D.G., Shirey, S.B., Carlson, R.W., Boyd, F.R., Pokhilenko, N.P., Shimizu, N., 1995b. Re – Os, Sm – Nd and Rb – Sr isotope evidence for thick Archaean lithospheric mantle beneath the Siberia craton modified by multi-stage metasomatism. Geochimica et Cosmochimica Acta 59, 959–977.
Pearson, D.G., Canil, D., Shirey, S.B., 2003. Mantle samples included in volcanic rocks: xenoliths and diamonds. Treatise in Geochemistry. In: In: Carlson, R.W. (Ed.), The Mantle, vol. 2. Elsevier, Amsterdam, pp. 171–276.
Pearson, D.G., Irvine, G.J., Ionov, D.A., Boyd, F.R., Dreibus, G.E., 2004. Re–Os isotope systematics and platinum group element fractionation during mantle melt extraction: a study of massif and xenolith peridotite suites. Chemical Geology 208, 29–59.
Philipidis, A., 1982. Experimental study of the serpentinization of Mg-Fe-Ni olivine in the presence of sulfur. Canadian Mineralogist 20, 567–574.
Reisberg, L., Lorand, J.-P., 1995. Longevity of sub-continental lithosphere from osmium isotope systematics in orogenic peridotite massifs. Nature 376, 159–162.
Richardson, S.H., 1986. Latter-day origin of diamonds of eclogitic paragenesis. Nature 322, 623–626.
Rudnick, R.L., Walker, R.J., 2009-this issue. Interpreting ages from Re–Os isotopes in peridotites. Proceedings of the 9th International Kimberlite Conference. Lithos 112S, 1083–1095.
Rudnick, R.L., McDonough, W.F., Chappell, B.W., 1993. Carbonatite metasomatism in the Northern Tanzanian mantle: petrographic and geochemical characteristics. Earth and Planetary Science Letters 114, 463–475.
Rudnick, R.L., McDonough, W.F., Orpin, A., 1994. Northern Tanzanian peridotite xenoliths: a comparison with Kaapvaal peridotites and inferences on metasomatic interactions. In: Meyer, H.O.A., Leonardos, O.H. (Eds.), Proceedings of the 5th International Kimberlite Conference: CPRM, vol. 1, pp. 336–353.
Ryan, C.G., Griffin, W.L., Pearson, N.L., 1996. Garnet geotherms: pressure-temperature data from Cr-pyrope garnet xenocrysts in volcanic rocks. Journal of Geophysical Research 101 (B3), 5611–5625.
Safonov, O.G., Vinograd, V.L., Wilson, D.J., Perchuk, L.L., Winkler, B., 2008. Potassium-bearing clinopyroxene: thermodynamic models and application to the barometry of mantle assemblages. 9th International Kimberlite Conference Extended Abstract No. 9IKC-A-00064.
Schmidberger, S.S., Francis, D., 1999. Nature of the mantle roots beneath the North American craton: mantle xenolith evidence from Somerset Island kimberlites. Lithos 48, 195–216.
Shaw, R.D., Meixner, T.J., Murray, A.S., 2000. Regional geophysical setting and tectonic implications of the mafic-ultramafic intrusions. Geology and Economic Potential of the PaleoProterozoic Layered Mafic-Ultramafic Intrusions in the East Kimberley, Western Australia: In: Hoatson, D.M., Blake, D.H. (Eds.), AGSO Bulletin, vol. 246, pp. 63–98.
Sheppard, S., Tyler, I.M., Griffin, T.J., Taylor, W.R., 1999. Paleoproterozoic subduction-related and passive margin basalts in the Halls Creek Orogen, northwest Australia. Australian Journal of Earth Sciences 46, 679–690.
Shirey, Harris, J.W., Richardson, S.H., Fouch, M., James, D.E., Cartigny, P., Deines, P., Viljoen, F., 2003. Regional patterns in the paragenesis and age of inclusions in diamond, diamond composition, and the lithospheric seismic structure of Southern Africa. Lithos 71, 243–258.
Shirey, S.B., Richardson, S.R., Harris, J.W., 2004. Integrated models of diamond formation and craton evolution. Lithos 77, 923–944.
Simakov, S.K., 2008. Garnet–clinopyroxene and clinopyroxene geothermobarometry of deep mantle and crustal eclogites and peridotites. Lithos 106, 125–136.
Simon, N.S.C., Carlson, R.W., Pearson, D.G., Davies, G.R., 2007. The origin and evolution of the Kaapvaal cratonic lithospheric mantle. Journal of Petrology 48, 589–625.
Smit, K.V., Shirey, S.B., Richardson, S.H, Gurney, J.J., le Roex, A.P., 2008. Off-Craton Ellendale diamonds, Kimberley Province, Australia. 9th International Kimberlite Conference Extended Abstract No. 9IKC-A-00176.
Sobolev, N.V., Pokhilenko, N.P., Yefimova, E.S., 1984. Diamond-bearing peridotite xenoliths in kimberlite and the problem of the origin of diamonds. Geologiya i Geofizika 25, 63–80 (in Russian).
Sobolev, N.V., Galimov, E.M., Smith, C.B., Yefinova, E.S., Maltsev, K.A., Hall, A.E., Usova, L.V., 1989. Comparative study of morphology, inclusions and carbon isotope composition of diamonds in alluvials of the King George River and Argyle Lamproite Mine (Western Australia), and of cube microdiamonds from Northern Australia. Geologiya i Geofizika 30 (12), 3–19.
Stachel, T., Harris, J.W., 2008. The origin of cratonic diamonds – constraints from mineral inclusions. Ore Geology Reviews 34, 5–32.
Taylor, W.R., Jaques, A.L., Ridd, M., 1990. Nitrogen defect aggregation characteristics of some Australian diamonds: time–temperature constraints on the source regions of pipe and alluvial diamonds. American Mineralogist 75, 1290–1310.
Trautman, R.L., 1999. The nature and genesis of microdiamonds. Ph.D. Thesis, University of Western Australia, 244 pp.
Tyler, I.M., Page, R.W., Griffin, T.J., 1999. Depositional age and provenance of the Marboo formation from SHRIMP- U-Pb zircon geochronology: implications for the early Paleoproterozoic tectonic evolution of the Kimberley region, Western Australia. Precambrian Research 95, 225–243.
Van Der Hilst, R.D., Kennett, B.L.N., Shibatani, T., 1998. Upper mantle structure beneath Australia form portable array deployment. In: Dooley, J., Goleby, J., van Der Hilst, B., Klootwijk, R. (Eds.), Structure and Evolution of the Australian Continent. In: AGU Geodynamics series. American Geophysical Union, Washington D.C, pp. 39–57.
Walter, M.J., 2003. Melt extraction and compositional variability in mantle lithosphere. In: Carlson, R.W. (Ed.), The Mantle and Core. Treatise on Geochemistry, The Mantle, pp. 363–394.
Westerlund, K.J., Shirey, S.B., Richardson, S.H, Carlson, R.W., Gurney, J.J., Harris, J.W., 2006. A subduction wedge origin for Paleoarchean peridotitic diamonds and harzburgites from the Panda kimberlite, Slave craton: evidence from Re–Os isotope systematics. Contributions to Mineralogy and Petrology 152, 275–294.
Wittig, N., Pearson, D.G., Webb, M., Ottley, C.J., Irvine, G.J., Kopylova, M., Jensen, S.M., Nowell, G.M., 2008. Origin of cratonic lithospheric mantle roots: A geochemical study of peridotites from the North Atlantic Craton, West Greenland. Earth and Planetary Science Letters 274, 24–33.
Worden, K., Carson, C., Scrimgeour, I., Lally, J., Doyle, N., 2008. A revised Palaeoproter-ozoic chronostratigraphy for the Pine Creek Orogen, Northern Australia: Evidence from SHRIMP U–Pb zircon geochronology. Precambrian Research 166, 122–144.
Zangana, N.A., Downes, H., Thirlwall, M.F., Marriner, G.F., Bea, F., 1999. Geochemical variation in peridotite xenoliths and their constituent clinopyroxenes from Ray Pic-French Massif Central: implications for the composition of the shallow lithospheric mantle. Chemical Geology 153, 11–35.